UNITED NATIONS UNIVERSITY
UNU-GTP
Geothermal Training Programme

Orkustofnun, Grensasvegur 9,
IS-108 Reykjavik, Iceland

Reports 2014
Number 16

BOREHOLE GEOLOGY AND HYDROTHERMAL ALTERATION MINERALOGY OF WELL MW-13, MENENGAI GEOTHERMAL FIELD, KENYA

Emily W. Kahiga
Geothermal Development Company - GDC
P.O Box 17700-20100
Nakuru
KENYA
ewangari@gdc.co.ke, w.kahiga@gmail.com

ABSTRACT

Rock cuttings provide a realistic picture on down-hole stratification and alteration. Therefore, the study of cuttings is essential in order to evaluate the dynamics of the geothermal system, such as permeability, temperature, size and depth of the reservoir. In this study, four different analytical methods (binocular, petrographic, microthermometry and X-ray diffractometry) were applied to analyse cuttings from well MW-13, located in the Menengai geothermal field, Kenya. This is a vertical production well, drilled to a depth of 2001 m. Well MW-13 was aimed at tapping NNW-SSE structures associated with the Molo and Solai Tectono-Volcanic Axes (TVA) which cut the Menengai caldera. Four rock types are encountered which include: trachyte (most dominant), tuff, pyroclastics and syenite. From litho-stratigraphic correlation of well MW-13 with other Menengai wells, several inferred faults have been identified, while a complicated tectonic scenario exists between some of the wells. The shallow section of the well is characterized by low-temperature hydrothermal alteration minerals which evolve to form high-temperature ones at greater depths. Four alteration zones, based on mineralogical assemblages, were identified: smectite-zeolite, quartz-smectite, epidote-quartz, and illite-wollastonite-actinolite-quartz. The uppermost 30 m section is unaltered. A comparison on the inferred alteration temperature, homogenization temperature (Th) and the boiling point curve shows that the system was in boiling conditions at some point in time. The measured temperatures do not reflect the current formation temperature. On correlating temperature logs to circulation losses, penetration rates (ROP), and lithological characteristics, eight permeable zones have been identified. The main sources of permeability are faults and lithological contacts. A brief comparison of clays in Menengai and Olkaria geothermal systems indicates that high-temperature clays appear at shallower depths in Olkaria wells than in Menengai wells. It is speculated that the different ages of the two systems are accountable for the dissimilarities noted.

1. INTRODUCTION

1.1 General information

Menengai geothermal field is one of the major high-temperature geothermal fields in Kenya, located within the Kenya Rift, in the East Africa Rift System (EARS). The EARS (roughly 6,000 km long) is an intracontinental ridge system (Chorowicz, 2005), and is mainly characterized by uplifting due to plumes beneath the rift system. At least two mantle plumes (Afar and Kenya) are recognized beneath the EARS (Rogers et al., 2000). The Kenya Rift encompasses the Turkana and Kenya rift zones (Bosworth et al., 1986) and is characterized by an active 500 km long continental extension which is 60-80 km wide (Strecker and Melnick, 2013). Leat (1984) describes Menengai as a Late Quartenary volcano, which is situated about 24 km south of the equator, 10 km north of Nakuru town, and defined by coordinates 35°04´S and 0°12´E (Figure 1). The field is characterized by a shield volcano with its highest peak at an elevation of 2278 m.a.s.l. and two fault systems: the Ol'rongai and the Solai (Figure 3). Geothermal resource exploration and development in Menengai field kicked off in 2009 and so far about 25 wells have been drilled. This project concentrates on the geological aspects of Menengai geothermal field; well MW-13 borehole geology is given the most attention. Well MW-13 is the thirteenth well, located within the caldera summit northeast of well MW-09 and directly north of well MW-10 (Figure 4). It is a vertical production well drilled to 2001 m depth, and was aimed at tapping NE-SW striking faults, as well as NNW-SSE structures associated with the Molo and Solai Tectono-volcanic axes (TVA). The well was also intended to supplement studies on the reservoir's physical characteristics such as rock permeability, storage capacity, boundary conditions, size and depth of the reservoir and chemical characteristics. It also provides data on hydrothermal mineralogy, subsurface structures, system capping and litho-stratigraphy, necessary for updating the Menengai geothermal conceptual model.

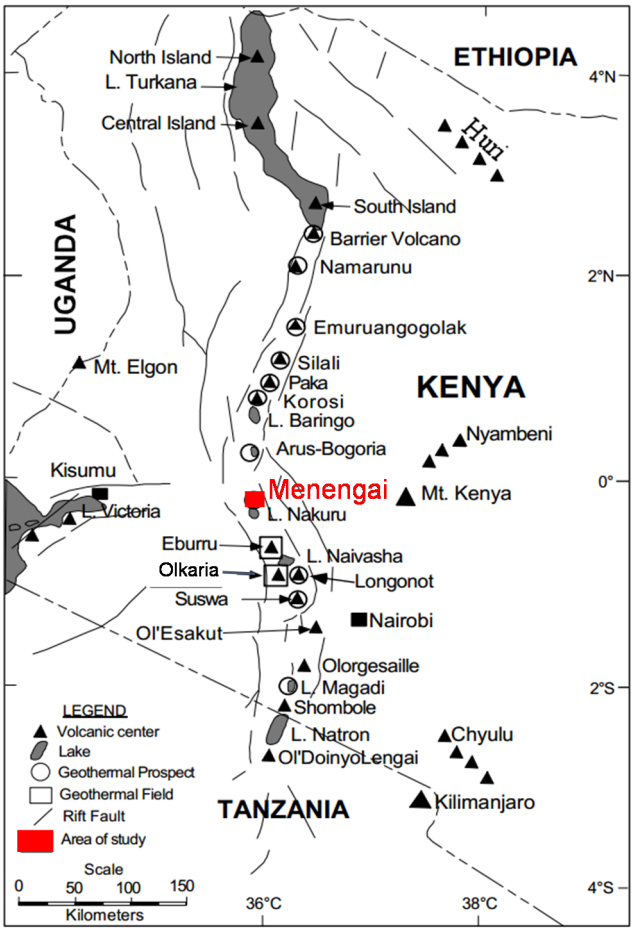

FIGURE 1: Map showing part of the EARS; Menengai caldera is located within the Central Kenya Rift (modified from Lagat, 2004)

1.2 Purpose of the project

This project study is aimed at critically evaluating the borehole geology and hydrothermal mineral alteration of Menengai well MW-13 via various lab analyses such as binocular and petrographic, among others. The project training is carried out as a partial fulfilment of a six months course in Borehole Geology at the United Nations University Geothermal Training Programme (UNU-GTP) in Iceland. The analyses are aimed at:

- Identifying and describing the different rocks encountered in well MW-13 and thereby updating knowledge on the litho-statigraphy and sub-surface structures in Menengai geothermal field;

- Studying the hydrothermal alteration minerals in the well with an aim of understanding better the water-rock interaction processes in the field, and thus providing clues on past and present conditions in the Menengai reservoir;
- Using the results to correlate well MW-13 with data from other Menengai wells with the aim of better characterizing the Menengai geothermal system with regard to its geophysical characteristics, including fault structures; and
- Attempting to compare the clays in Menengai wells with that of Olkaria wells.

1.3 Previous work in Menengai

Numerous studies have been carried out in Menengai, both in the past and present, with different aims, ranging from geological, scientific research, academic reasons, government interests, geothermal exploration, and so on. Dixey (1946) studied the erosion and tectonics in the East Africa System in which Menengai is located. McCall (1957) more specifically reviews the Menengai caldera and suggests a Krakatoan type of caldera collapse, while McCall (1967) describes the geology of the Nakuru-Thomson's Falls-Lake Hannington area and, hence, that of Menengai volcano. Jones (1975; 1985) further discusses the geological evolution of the Menengai trachytic caldera, whereas Jones and Lippard (1979) attempted to estimate the age of Menengai rocks. Leat (1984 and 1991) extensively discusses the geological and volcanological evolution of the Menengai volcano and concludes that it developed during three major phases.

Early Menengai geothermal exploration work was carried out by Geotermica Italiana Srl. (1987) when a reconnaissance survey for the geothermal resource took place in the area. Tole (1996), in his review on geothermal energy research in Kenya, lists the Menengai crater as one of the prospects and proposes more research to evaluate the field's potential. More geothermal exploration work at the Menengai-Ol'banita area was conducted by BGR (2009). In 2004, KenGen carried out detailed surface geothermal exploration, which confirmed that Menengai could host a viable geothermal resource for exploitation (KenGen, 2004). Other previous studies (Simiyu and Keller, 1997; 2001; Mariita and Keller, 2007) explain the presence of a high gravity anomaly along the rift volcanic centres and interpret them to be a result of a shallow magma chamber and dykes along the rift axis. GDC (2010) conducted intense integrated geothermal mapping in the Menengai prospect area which confirmed previous work. The study resulted in a clearer citation of the major geological structures and geothermal manifestations in the prospect area while the geophysical measurements confirmed the presence of a heat source beneath the Menengai caldera. Additionally, gas geothermometry estimated reservoir temperatures to be in excess of 250°C (Kipchumba, 2013). The intense studies were used to site exploration wells, and exploratory drilling started in 2011. Since then, numerous studies have been progressively carried out to re-evaluate the geothermal system. For instance, several studies on completed wells have been carried out (Kipng'ok, 2011; Gichira, 2012; Lopeyok, 2013). In addition, more recent studies (Wamalwa, 2011) confirm the presence of a heat source (at about 7 km depth), as well as high porosity and permeability. Further structural mapping has recently been carried out (Strecker and Melnick, 2013), aimed at re-evaluating the Nakuru area in light of the ongoing geothermal exploration.

2. GEOLOGY AND STRUCTURAL SETTING

2.1 Regional geology and tectonic setting

The Kenyan segment of the East African Rift System (EARS) is the eastern branch of the Africa Rift System; the other two branches include the western and southeastern. The Kenya rift system extends from Lake Turkana in the north of Kenya, to the north of Tanzania near Lake Natron (Figure 1). Hetzel and Strecker (1994) and Smith and Mosely (1993) concluded that rifting was initiated by rift faults within the Late Proterozoic basement of the Mozambique belt, adjacent to the eastern margin of the

Tanzania craton. Active faulting started during the Cretaceous period, around 119 to 120 Ma, resulting in rapid subsidence and thick deposition along the Sudan-Kenya NW-SE trending troughs (Guiraud et al., 2005). Folding, as explained by Ali Kassim et al. (2002), then followed due to dextrial transpression, forming the ENE–WSW fold belt. Uplifting, rifting, folding and thrusting continued during the Paleocene times (Tole, 1996; Guiraud et al., 2005; Guiraud and Bosworth, 1999), shortly followed by regression in the Early and Middle Eocene. The last stage in the development of the Rift (from Late Eocene to Late Oligocene) was characterized by strong magmatic and tectonic changes (Guiraud et al., 2005; Chorowicz, 2005; MacDonald, 2003), as well as domal uplifting of about 300 m (Kipchumba, 2013). From Early Miocene to Pliocene, the collision between the African-Arabian and Eurasian plates intensified (Guiraud et al., 2005; Tole, 1996), leading to intense volcanic eruptions, uplifting and subsequent faulting episodes. Baker and Wohlenberg (1971) described the basaltic, phonolitic and trachytic volcanism that followed during the Late Pliocene, while uplift and graben faulting resulted in the present day rift structures. Baker et al. (1988) suggested that this faulting was triggered by a convecting mantle, opening up fractures which served as conduits for Quaternary volcanic activity and the development of many large shield volcanoes of silicic composition along the rift axis. Menengai is one of the shield volcanoes among others, such as Olkaria, Eburru, Suswa, Longonot, Korosi, Paka, Silali, Emuruangogolak, and the Barrier Complex (Figure 1).

2.2 Geology of Menengai volcano

The Menengai caldera is located north of Lake Nakuru, and within the Kenyan rift (Figure 1). Leat (1991) describes that trachytic magma eruptions have continuously been recorded for the last 6.2 Ma. Figure 2 shows the surface geology and various geological structures of Menengai caldera. The oldest exposed rock unit is the Mau Tuffs (Leat, 1991), found to the west of Lake Nakuru, and the Subukia Trachyphonolite (Leat, 1983) located on the eastern flank (Figure 2). The subsequent volcanic unit is marked by the Pliocene Bahati Trachytes and Tuffs (5.1-2.0 Ma) which are highly faulted. The Early Pleistocene Limuru Trachytes (1.96 ± 0.04 Ma) followed and are exposed in the area in a scattered manner (Baker et al., 1988; Crossley, 1979). According to Leat (1991), the evolution of the Mbaruk Basalt and Trachyte (about 1 Ma) followed, and are mainly visible at the southern part of Menengai (Figure 2).

The youngest group of volcanic rocks is associated with the eruption of two ignimbrites and the collapse of the 77 km^2 Menengai caldera (Leat, 1984). According to Leat et al. (1984), Menengai caldera is part of a trachytic central volcano of late Quaternary age and its volcanic activity started just before 0.18 Ma. Macdonald et al. (2011) further explained the geological evolution of the Menengai caldera. Its onset was a shield-building phase, also termed Pre-caldera activity by Leat (1984). The eruption of two voluminous ash-flow tuffs (about 29 km^3) followed, each preceded by major pumice falls. Two caldera-forming events (Syn-caldera activity) then followed (29 ka and 8 ka, respectively), accompanied by an eruption of a 20-30 km^3 ash-flow. Post-caldera activity is largely marked by a series of lava flows (at least 70 flows) (Leat, 1984; Mibei and Lagat, 2011). Strecker and Melnick (2013) established that volcanic deposits related to Post-caldera activity are exposed in the immediate vicinity of the caldera.

2.3 Structural setting of Menengai volcano

Structures in the Menengai volcano are poorly exposed due to the intensive cover of recent lavas on the caldera floor. Nevertheless, numerous studies (GDC, 2010; KenGen, 2004; Simiyu and Keller, 1997; Strecker and Melnick, 2013; Leat, 1984) have assessed various structures of significance in this field and the surroundings. On a regional scale, Menengai caldera is affected to the north and south by NNE striking normal faults, while the western section appears unaffected. The major structures are as discussed below.

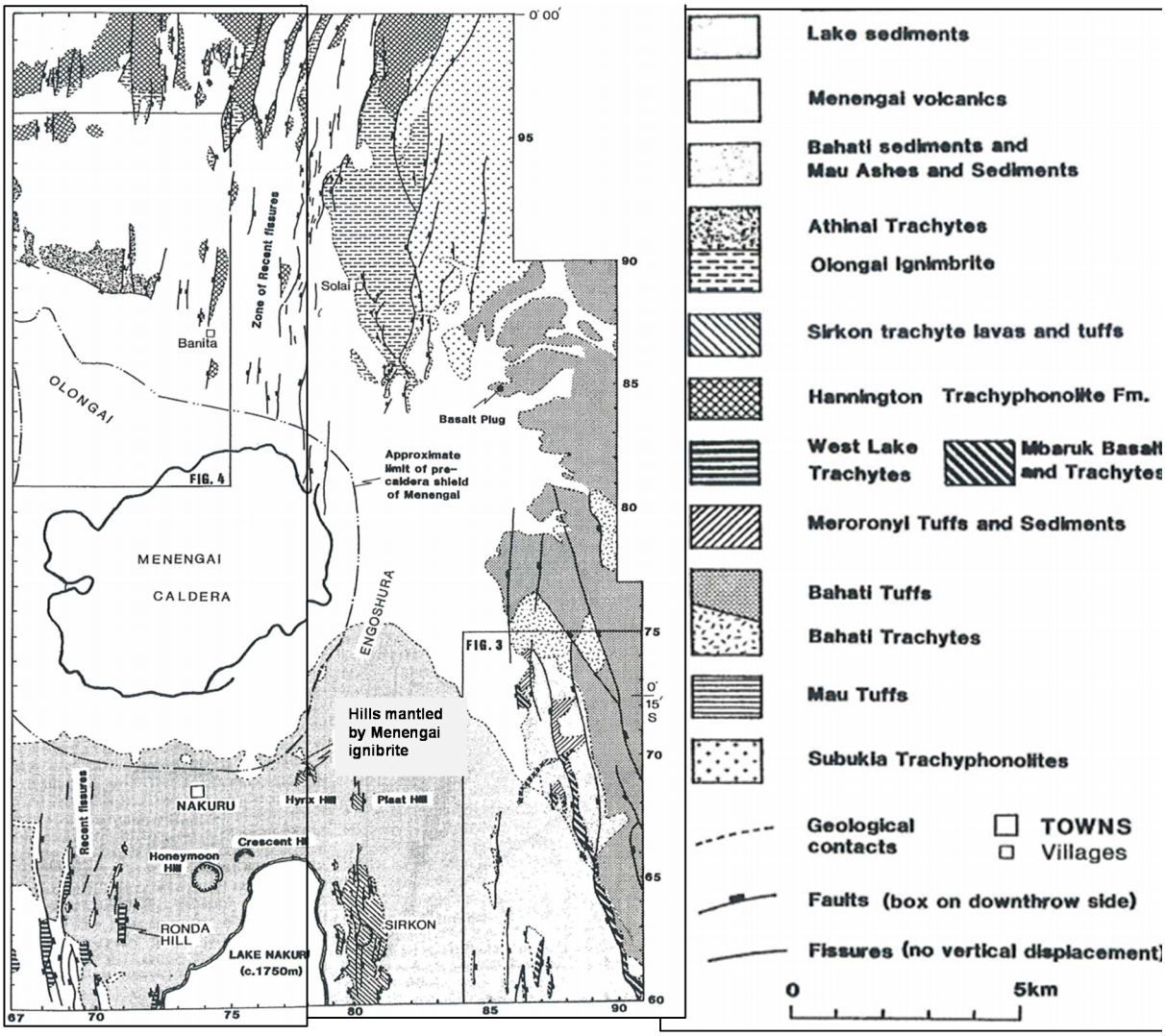

FIGURE 2: Geological map of Nakuru area, showing the surface geology of Menengai caldera, its outline, faults, fissure zones and other structures; the Menengai volcanics are undifferentiated to emphasize the geology of older formations (modified from Leat, 1991)

2.3.1 Ol´rongai structural system

The Ol´rongai structural system (Figure 3) forms part of the larger Molo tectono-volcanic axis (TVA (Geotermica Italiana, 1987). Mibei and Lagat (2011) and Mibei (2012) deduced that the Ol´rongai system is associated with a system of young NNE-SSW striking normal faults and fractures along which volcanic eruptions have taken place. Most likely this explains the presence of aligned craters and fumaroles on the surface along this fault zone, as shown by Strecker and Melnick (2013) and Lynne et al. (2006). Leat (1984) associates the Ol´rongai system with a NW-SE trending ridge where Pre-caldera rock units are seen; therefore, the Ol´rongai fault system should be older than the Solai system which cuts into the caldera on the NNE side.

2.3.2 Solai Tectono-volcanic axis and Makalia fault system

The Solai TVA system (Figure 3) is a narrow (4 km wide on average) graben, defined by a NNE-SSW orientation through Lake Solai (Figure 2) (Mibei and Lagat, 2011). The Solai TVA is part of the Solai graben which Leat (1984) interpreted as being continuous with a swarm of very young faults. The Solai fault system is younger than the Menengai caldera as it cuts the caldera wall to the north, disappears below the pyroclastic cover, and reappears on the SW corner of the caldera. In the same context,

Strecker and Melnick (2013) confirmed that a similar NNE-SSW aligned lineament can be traced farther south along the caldera floor; the lineament is characterized by a 1 km wide NNE oriented volcano-tectonic zone which hosts NNE-SSW elongated eruptive centres. This suggests that the Makalia fault system (Figure 3) is an extension of the Molo system, and is further inferred by Strecker and Melnick (2013), proposing that the two systems, Solai and Makalia, may coincide, thus, forming an extensional fault system.

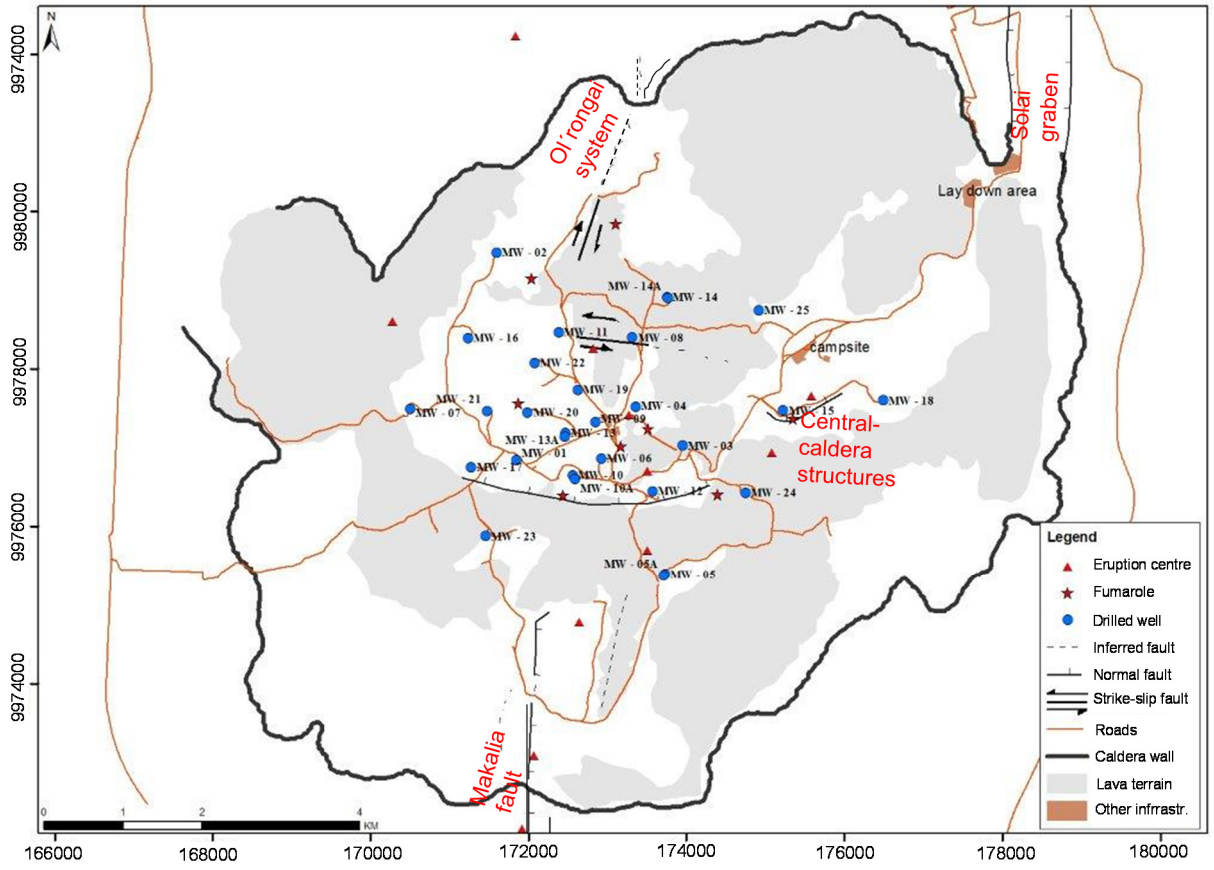

FIGURE 3: Structural map of Menengai geothermal field
(modified from Strecker and Melnick, 2013)

2.3.3 The Menengai caldera and ring faults

The Krakatau-style Menengai caldera is elliptical in shape, with embayed walls up to 300 m high and measures approximately 12 × 8 km (Leat, 1984). Apart from the Post-caldera lavas that cover the caldera floor, the circular rim of the Menengai caldera is well-preserved. Nevertheless, the ring structure has been disturbed by the Solai system on the northeast side, implying that the ring fault is older than the Solai system. Additionally, recent Post-caldera lava flows from eruptive centres have spread over the caldera wall on the southern side (Strecker and Melnick, 2013). An embayed ring fracture is evidenced by the presence of surface expressions of faults and randomly spaced Post-caldera vents close to the caldera wall (Leat, 1984; Strecker and Melnick, 2013).

2.3.4 Central-caldera structures

According to Strecker and Melnick (2013), there are numerous linear features oriented either ESE-WNW or E-W, in the central area of the Menengai caldera. Leat (1984) suggests a region of weakness in the central part through which magma easily ascended onto the surface. The central-caldera structures display a different orientation from that of feeder-dykes. Strecker and Melnick (2013) attributed this to doming which is associated with magma intrusions. Resistivity studies by Wamalwa (2011) and Simiyu

and Keller (2001) confirm magma injection and a low-resistive zone along the central-caldera features. Additionally, these features are characterized by numerous fractures with aligned fumaroles (Figure 3), some of which are active and sulphurous.

3. SAMPLING AND ANALYTICAL METHODS

3.1 Sampling

Rock cuttings provide a realistic picture of down-hole stratification and alteration and thus, are useful for characterizing down-hole alteration temperatures and composition (Marks et al., 2009). During drilling, cuttings were collected at a 2 m interval depth for lithologic logging. A binocular microscope was used to analyze the cuttings at the rig site, aimed at developing an initial litho-stratigraphy and estimating down-hole temperatures by using alteration mineralogy. The resulting data were applied in defining the casing depth and directing drillers on geotechnical aspects, especially with regard to the type of formation, fracturing, temperature, etc. Sample portions were eventually taken to the ISOR (IcelandGeoSurvey) laboratory for detailed analysis. Binocular, petrographic, X-ray diffraction and fluid inclusion studies, under proper and ample guidance, were also carried out on the cuttings at ISOR.

3.2 Analytical Methods

3.2.1 Binocular microscope analysis

An Olympus SZX12 stereo microscope was used to critically investigate the physical characterstics of the rock cuttings such as the rock type, color, texture and grain size, rock fabric, primary and secondary alteration mineralogy. Other various geological and structural aspects were also studied using the cuttings such as intrusive activity, permeability and feeder zones, mineral sequences, porosity, vein fillings, litho-stratigraphic boundaries and the grade of alteration. Rock cuttings, placed in sample holder boxes, were sufficiently wetted to enhance reflectivity, and then mounted on the stage of the binocular microscope. Careful inspection of the cuttings was then carried out and the observations were noted down for interpretation. During the binocular analysis, representative samples, based on the noted observations, were carefully selected and prepared for advanced scrutiny by using other analytical techniques.

3.2.2 Petrographic microscope analysis

A LeitzWetzlar petrographic microscope was used to study thirty thin sections. The analysis was aimed at confirming the various observations made during the initial binocular studies such as the rock type, texture, porosity and alteration minerals. Additional observations made included recognizing alteration minerals which were not identifiable using a binocular microscope and defining mineral sequences, which are rarely distinguished in the cuttings by binocular analysis.

3.2.3 X-ray diffractometer analysis

This technique is mainly used for identification of clay minerals, which is important in assessing alteration temperatures in geothermal systems. Clay minerals are known to have diverse mineralogy and crystal structures, thus, are not easily distinguishable by microscopic analysis. Thirty six samples were chosen from representative depths, and prepared for XRD studies. A Bruker AXS, D8 Focus diffractometer (Bragg-Brentano goniometer) was used, with Ni-filtered Cu kα radiation at 1.54 Å wavelength at 40 mA and 40 kV, with fixed 0.5° (1 mm) divergence and receiving slits and NaI scintillation counter with a 0.2 mm detector slit. The recorded peaks and patterns were processed and identified by using both the *JADE* software (Materials Data, Inc.) and the Powder Diffraction File (PDF) database of the International Centre for Diffraction Data (ICDD).

3.2.4 Fluid inclusion analysis

Any process that interferes with the growth of a perfect crystal may cause trapping of primary fluid inclusions. Secondary fluid inclusions are, however, trapped along healed cracks. Analysis of fluid inclusions, also known as microthermometry, is the observation of various phase changes in fluid inclusions under controlled conditions of heating and cooling (Harvey and Browne, 2000). At ambient temperatures, all types of inclusions contain a liquid aqueous solution and a gas bubble (Lagat, 2004). The inclusion is heated and the homogenization temperature (Th) measured. Microthermometry studies help in deciphering the temperature of past geologic events such as tectonics and uplifting. Roedder (1984) compares fluid inclusions to a self-contained geothermometer preserving a specific temperature of a past event. Thus, fluid inclusion analysis objectively gives a simple specific history and prediction on the behaviour of a geothermal system. For this study, two grains of secondary qurtz were carefully collected from a representative depth range. Each grain, one at a time, was then slowly heated on a Linkam THSMG 94 freezing and heating stage. The Th was measured for further interpretation. A total of 71 inclusions were analysed.

The data acquired from all of the above analyses were assimilated and compiled using LogPlot 2007 (RockWare Inc., 2007), a software which is beneficial in correlating and interpreting geological and geotechnical data.

4. BOREHOLE GEOLOGY

As described earlier, well MW-13 is near the Menengai caldera summit, northeast of well MW-09 and directly north of well MW-10 (Figure 4).

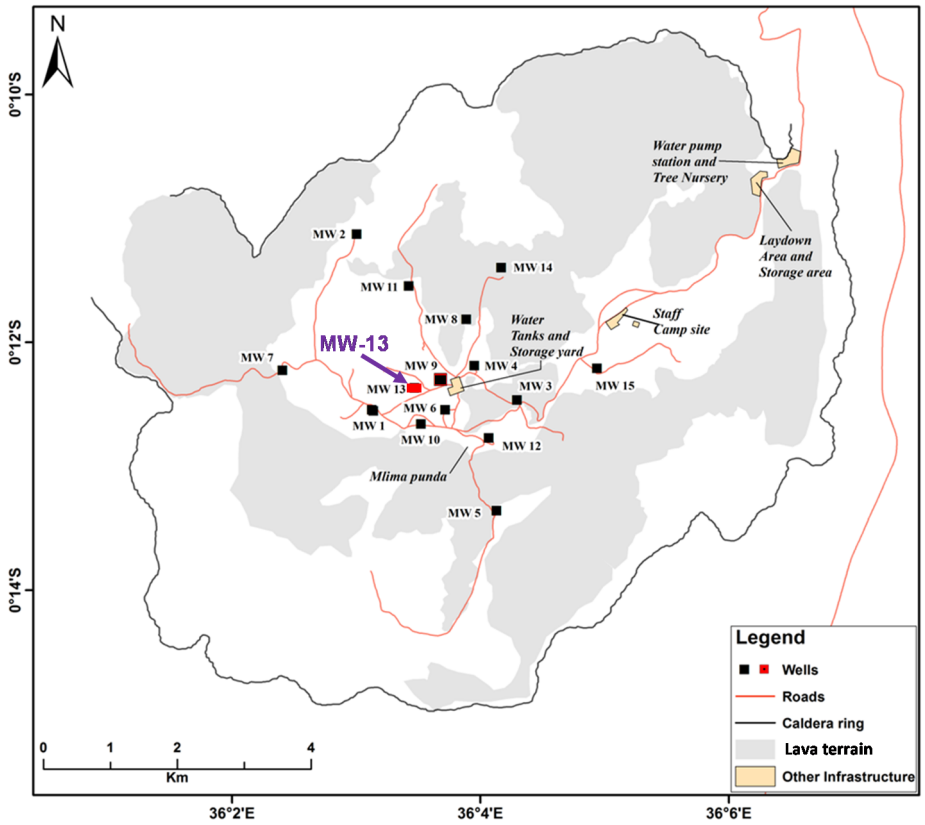

FIGURE 4: Location of well MW-13, highlighted in red colour

4.1 Drilling of well MW-13

MW-13 was spudded on 1st January 2013 and completed on 8th June, 2013; the well was drilled to a depth of 2001 m CT (Cellar Top). A total of 159 days were spent on this well operation: 81 days on drilling while 78 days on downtime, attributed mainly to repairs on a damaged crown block (Figure 5). Four different drilling phases (Figure 5), each with a different casing size, were employed as described below. Note that all referred depths are as measured from the cellar top (CT).

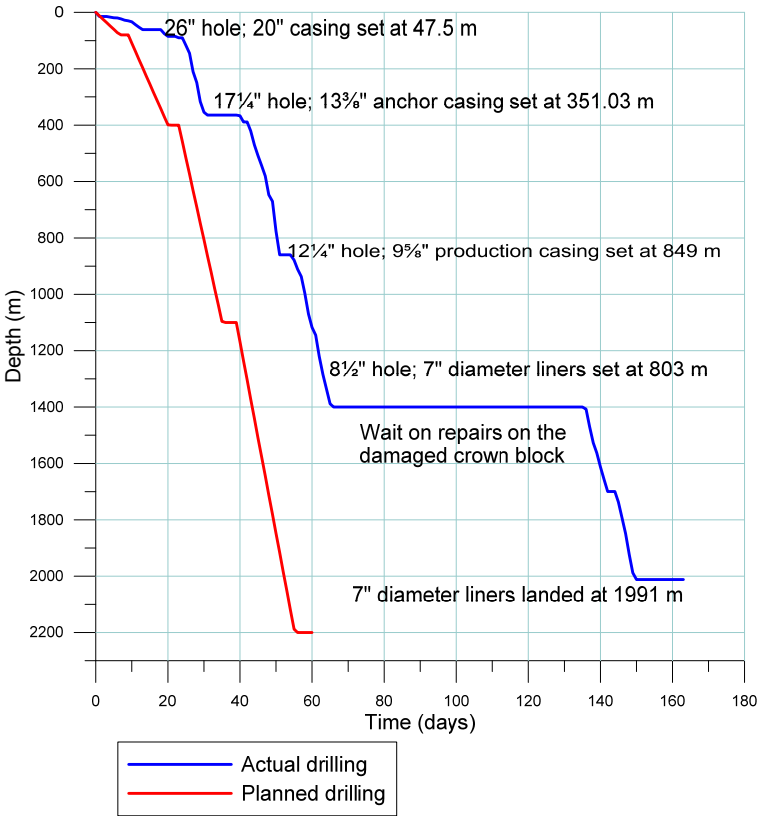

FIGURE 5: Graphical representation of well MW-13 drilling progress

Phase one, 26" hole: The 26" hole was drilled to a depth of 50.30 m, with mud and water as drilling fluids. Total loss of circulation was encountered at a depth of 7.5 to 8.5 m where a 6 m^3 cement plug of density 1.9 g/cm^3 was completed. Cement returns were received on the surface after primary cementing, after which 2 backfills were performed. A total of 83.87 tons (cement plugs inclusive) of neat cement were used for cementing the 20" surface casing, which was set at 47.5 m.

Phase two, 17¼" hole: Drilling of this section was done to a depth of 353.1 m. This zone was characterized by a total loss of circulation and, hence, LCM (Loss Circulation Material) was used to cure the loss zones and regain circulation. At 120 m, curing of losses failed completely, leading to drilling blind to a casing depth of 353.1 m. Wiper trip was conducted and the 13⅜" anchor casing was set at 351.03 m on 1st February, 2013. A total of 147.88 m^3 cement slurry with a density of 1.72 to 1.85 g/cm^3 was used before cement was received on the surface.

Phase three, 12¼" hole: Drilling of this section of the hole started on 4th February, 2013, to a total depth of 859 m. The well was logged at 355 m showing 1.0° inclination. Mud was used as the drilling fluid in this segment with full returns received through to 849 m depth, at which the 9⅝" production casing was set on 21st February, 2013. Primary cementing was done with two backfills before returns were received on the surface. A total of 6.6 tons of cement at 1.72 g/cm^3 density was used in this zone.

Phase four, 8½" hole: This final part of the hole was drilled using aerated water and foam, to a depth of 2001 m. Drilling progressed successfully, after one bit change at 1106 m, until 7th March, 2013, at 1389 m depth, where a travelling block struck on the crown block during POOH (Pulling Out Of Hole) to change the 8½" bit and stabilizer sleeve, damaging three sheaves. Repairs on site were not successful; therefore, the damaged sheaves were extracted and taken away for maintenance. Drilling resumed on 17th May, 2013, with alternating total loss to partial circulation. Successful drilling was conducted to 30th May, 2013, with wiper trip being performed up to the casing shoe prior to running liners. On 1st June 2013, 7" diameter liners were run in hole with 102 joints of slotted liners and 2 plain liners. The liner was landed at 1991 m with the top set at 803.15 m. Well logging commenced on 1st June 2013, whereby a dummy was run but encountered an obstruction at 1044 m. This led to the use of 3½" diameter

drill pipes, enabling a successful tool run. The 3½" diameter drill pipes were POOH and logging was done again with a clear dummy run to 1979 m. A SFTT (Static Formation Temperature Test) and a pressure test were executed successfully. The well was capped with a class 900 master valve on 8th June, 2013.

4.2 Stratigraphy

Well MW-13 stratigraphy is dominated by trachyte lavas and some intermittent tuff intercalations. Other minor rock formations include pyroclastics and syenitic intrusions. The lithological sequence is described below and shown in Figure 6; rock descriptions are based on the analysis of cuttings, supported by petrographic and XRD analyses.

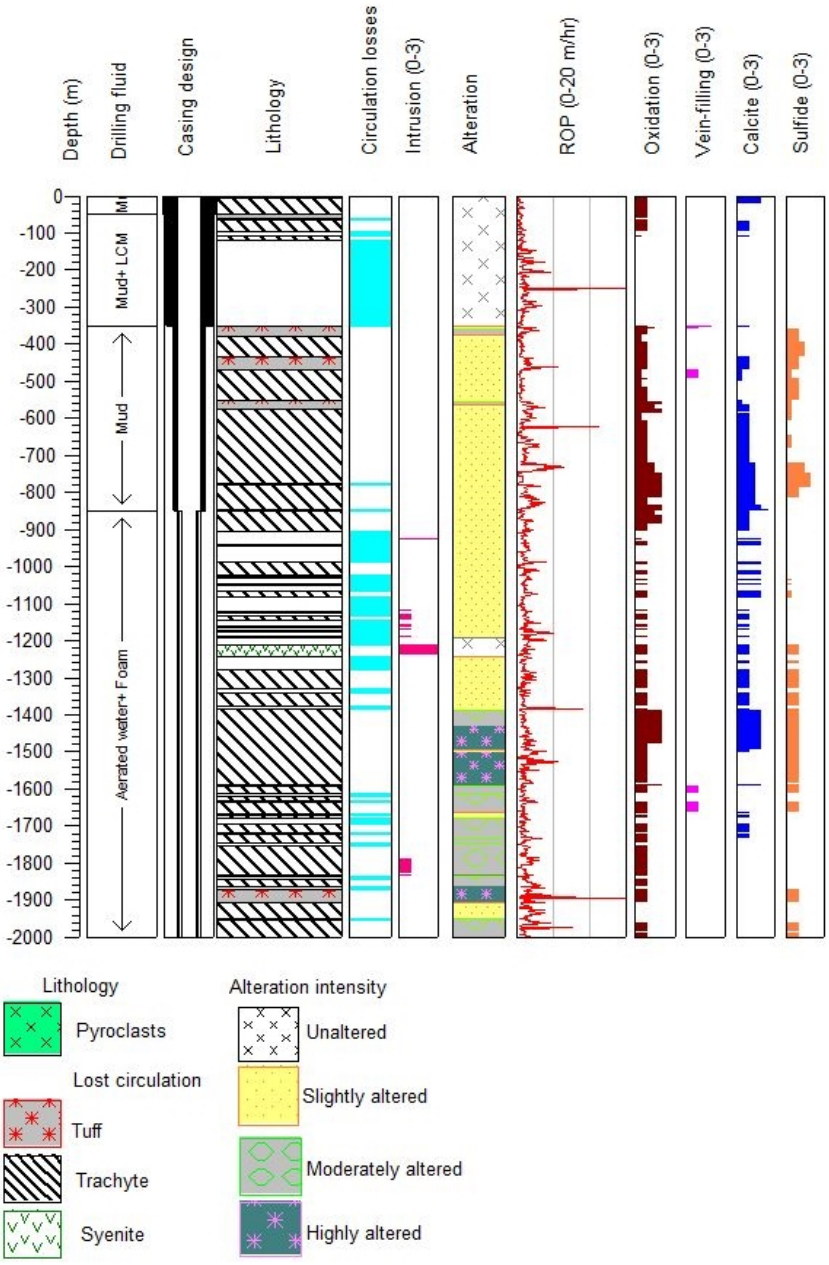

FIGURE 6: Well MW-13 lithology, the intensity of alteration, oxidation, vein-infilling and penetration rates

Pyroclastics are clastic rocks primarily composed of volcanic materials such as unconsolidated ash and bombs. Pyroclastics in well MW-13 are encountered at shallow depth (top 4 m); surface alteration, mainly oxidation, is noted at this depth range (Figure 6). In binocular microscopy, the volcanic unit appears as grey to brownish grey pumice lapilli particles, obsidian, glass and lithics of trachytic composition. Pyroclastics further appear as a thin sheet at 1590 to 1592 m. At shallower depths, the pyroclastic formation resembles Post-caldera lavas as described by Leat (1984), probably originating from eruptions within the caldera. The deeper sequence signifies an old land surface, appearing as a reddened oxidized soil horizon. In the deeper pyroclastic formation, sulphides, calcite and clay alteration and oxidation are notable in the cuttings.

Trachyte occurs alternating with tuff and syenite at 50 m and 1198 m, respectively, and appears till the bottom of the well (Figure 6). It is the dominant rock type in well MW-13, with minor tuff intercalations at greater

depths. The rock colour varies from light to dark grey and grey to greenish/brownish grey, fine to medium grained, and predominantly porphyritic. The variation in crystallinity (different rock textures such as fine to medium grained, porphyritic, phaneritic, aphanitic) is attributed to the age differences in the evolution of Menengai caldera, as demonstrated by Leat (1984 and 1991). Therefore, the age of the trachyte in well MW-13 ranges from Pre- to Syn- and Post-caldera. Additionally, the cuttings show well-elongated phenocrysts of sanidine, as well as prismatic phenocrysts of pyroxenes. The matrix is composed of flow oriented feldspar grains in a fine to medium grained groundmass. At greater depth, in thin sections, nepheline is notable as colourless to greenish, stubby mineral grains with no cleavage. The alteration of this formation is highest at contact boundaries, and its primary minerals are altered to both high and low temperature secondary minerals.

Tuff: The tuff layers in well MW-13 divide trachyte lavas, thus acting as marker horizons separating Pre- and Post-caldera volcanic activities. Therefore, tuff mainly relates to Syn-caldera activity in Menengai. The rock type was first observed at 50 m and later appears intermittently to the bottom of the well, intercalated with trachyte and syenitic intrusions. Tuff is recognized in well MW-13 by its frothy, vesicular and aphyric texture, as well as felsic colours such as brownish grey. The vesicles are mainly filled with calcite, clays, pyrite, quartz, and actinolite at high temperatures. A tuff layer observed at 1872 to 1906 m has high permeability, high ROP, contains sulphides and shows poor crystallinity, similar characteristics as observed in a deep tuff horizon in wells MW-04, MW-06 (Mibei, 2012) and MW-09 (Lopeyok, 2013) and, thus, believed to be related.

Syenite appears as a white coarse-grained, porphyritic and fresh formation with prismatic pyroxene grains. The formation in well MW-13 occurred as thin lenses irregularly intercalated with trachyte from 1118 m. The syenitic formation zone was characterized by frequent losses; the formation is hard and compact as deduced from the low penetration rates during drilling, and very low sulphide content. Syenite in well MW-13 is consistently associated with high temperature minerals like epidote, albite, actinolite and wollastonite. This signifies contact alteration resulting from the hot intrusion. The appearance of empty cavities in cuttings is also of key interest, probably confirming the aforementioned indication of localized geothermal activity. The syenitic intrusion probably correlates to the proposed existence of an axial intrusion beneath Menengai volcano (Leat, 1984).

4.2.1 Lithology of well MW-13

0-4 m: Pyroclastics. Fine to medium grained heterogeneous rock fragments that show varied colours such as green, black, brown, grey and reddish. A vesicular frothy texture was also noted. Oxidation, attributed to surface alteration due to rock interaction with air and water, and minor calcite were noted in the cuttings.

4-50 m: Medium-grained trachyte. Relatively fresh dark greyish black lava, equigranular, medium grained lava that is feldspar porphyritic, with easily notable pyroxene and sanidine phenocrysts. At 38 m, cuttings exhibit a peculiar greenish tinge. Alteration is noted by oxidation, calcite, amorphous silica, chalcedony and zeolites.

50-62 m: Tuff. A thin layer of brownish grey, vesicular and frothy cuttings. A few grains of sanidine porphyritic lava were also notable. Minor oxidation, amorphous silica, zeolites and pyrite define alteration in this zone.

64-352 m: Fine-grained trachyte. Black grey to felsic brownish grey, fine grained feldspar porphyritic lava which is fairly unaltered. Some vesicular cuttings were also noted. Alteration in this zone is defined by minor oxidation, clays, calcite and zeolites. The zone is permeable as deduced from frequent loss of cuttings at 68-74; 98-108; and 120-352 m.

352-380 m: Tuff. Brownish vesicular tuff fragments which exhibit moderate alteration. Greenish minerals and pyrite disseminations were notable on the surfaces and in the vesicles. Minor brownish

grey to green, fine-grained trachytic lava were also notable. Oxidation, calcite, clays and pyrite alterations dominate this well section to about 722 m depth.

380-434 m: Fine-grained trachyte. Greenish grey to white fine grained, feldspar porphyritic lava. Pyrite infillings and some minerals being slightly altered to brown and greenish clay minerals were noted.

434-472 m: Tuff. Brownish to greenish grey vesicular and frothy lava. Vesicles are mainly filled with clays and some oxidized minerals. Elongated sanidine phenocrysts were also notable.

472-552 m: Fine-grained trachyte. Greenish grey to black, relatively fresh, fine grained porphyritic lava, rich in elongated sanidine and pyroxene phenocrysts. Pyrite alteration decreased at 494 m.

552-576 m: Tuff. Greenish brown, vesicular and frothy rock fragments. An increase in clay alteration was noted at 552-556 and decreased at 556-564 m. At 564-576 m, the cuttings were reddish brown, quite compacted, aphanitic and exhibit assorted rock fragments with conspicuous sanidine phenocrysts. Minor trachytic cuttings were also notable.

576-982 m: Fine-grained trachyte. Greenish black to brown fine grained porphyritic lava which is fairly fractured, with well pronounced feldspar and pyroxene phenocrysts; fluid inclusions evident in some of the feldspar phenocrysts. At 778-786 and 848-850 m, some cuttings show a peculiar blue green tinge on the surfaces. Minor tuff fragments intermittently noted in the well segment, which is also characterized by frequent loss of circulation at 774-778; 846-850; 906-940; and 944-982 m. Chalcopyrite embedded in the groundmass was noted from 722 to 846 m.

982-1198 m: Fine-grained trachyte. Light grey porphyritic, relatively unaltered and fractured lava with well pronounced sanidine and pyroxene phenocrysts embedded in a fine grained groundmass. The common yellow green epidote colour was noted at 992 m and 1012 m. Albite, sphene and MLC started showing up in this depth range. Minor syenite cuttings were also noted. From 1124 m, pyroxene phenocrysts were more conspicuous and elongated. This zone is characterized by intermittent losses at 984-988; 996-998; 1012-1014; 1024-1028; 1030-1036; 1038-1042; 1044-1048; 1052-1066; 1070-1072; 1080-1082; 1084-1106; 1108-1118; 1120-1122; 1126-1132; 1146-1160; 11661172; 1176-1188; 1192-1198 and 1200-1208 m.

1208-1256 m: Syenite. White, coarse grained, quite fresh rock formation exhibiting prismatic grains of pyroxene, embedded in a feldspar-rich groundmass. Well distinguishable nepheline crystals were observed in thin section. Calcite-filled veins were also present. Epidote, pyrite and albite alteration was observed. This zone is described by intermittent losses occurring at 1208-1210; 1234-1236; 1240-1242; 1244-1250, and 1252-1256 m.

1256-1478 m: Fine-grained trachyte. Greyish black, fine grained feldspar porphyritic lava that is fairly unaltered. At 1384 m, a peculiar bluish mineral deposit in vesicular fragments was noted. Pyrite embedded with thin fibrous greenish grey and whitish crystals of actinolite and wollastonite, respectively, were noted. Intermittent losses occurring at 1258-1260; 1262-1280; 1310-1312; 1328-1340; 1376-1384; 13961398 and 1400-1402 m.

1496-1590 m: Medium-grained trachyte. Greenish grey to brown, medium grained pyroxene porphyritic lava that is fairly altered and shows prismatic and elongated pyroxene crystals. Some cavities that had not been filled were noted at 1562 m. At 1594 m, some cuttings were altered into bluish minerals. From 1496 to 1592 m, relatively high alteration was noted by the presence of minor calcite, clays, actinolite, wollastonite, pyrite and quartz.

1590-1592: Pyroclastics. Fine to medium grained assorted rock fragments that show a variety of colors such as green, black, brown, grey and reddish. A vesicular frothy texture was also noted. Circulation losses were encountered at 1518; 1524; 1544; 1572; 1578; 1584 and 1590 m.

1592-1832 m: *Medium-grained trachyte.* Greenish grey to brown medium grained pyroxene porphyritic lava, fairly altered, shows prismatic and elongated pyroxene crystals. Higher alteration at 1592 to 1734 m was marked by minor calcite, clays, actinolite, wollastonite, pyrite and quartz. However, alteration significantly diminished from 1734 to 1832 m. Circulation losses were observed at 1604; 1608; 1612-1620; 1630-1634; 1638; 1662;1692; 1666-1670; 1678-1690; 1692-1696; 1712; 1718-1722; 1744-1754; 1758; 1772 and 1808 m.

1832-1842 m: Syenite. Whitish grey, coarse grained, relatively fresh formation, with pyroxene in a feldspathic groundmass. Circulation losses were noted at 1836-1842 m.

1842-1872 m: Fine-grained trachyte. Greenish grey, fine grained, fairly fractured lava with notable sanidine and pyroxene phenocrysts. Decreased effective permeability was indicated by reduced alteration and the absence of sulphides. Random reddish brown spotting was noted at increasing depth and a circulation loss zone was noted at 1864-1872 m.

1872-1906 m: Tuff. Greenish brown, aphanitic vesicular, reasonably altered lava, mixed with minor crystalline cuttings. Most of the vesicles are filled by clays and some tiny quartz crystals. The formation is medium soft and permeable as deduced from high penetration rates.

1906-2000 m: Medium-grained trachyte. Whitish brown to greyish green, fine to medium grained porphyritic lava that is relatively unaltered. Some cuttings of white fresh lava with mafic phenocrysts were also present. Some of the cuttings appear fresh and highly compacted, probably indicating diminishing effective permeability. However, at 1962-2000 m, the cuttings appeared reasonably altered to greenish clay minerals, with some minor alteration minerals also visible, such as wollastonite, actinolite and sulphides. Some cuttings demonstrated an unusual blue green tinge at 1958 m. Circulation losses were encountered at 1950-1954; 1984-1988 and 1990-1992 m.

4.3 Litho-stratigraphic correlation of well MW-13 and other wells

The stratigraphy of wells MW-13, MW-01 (GDC, 2013a), MW-04 and MW-06 (Mibei, 2012) and MW-09 and MW-12 (Lopeyok, 2013), has been interrelated to understand better the Menengai marker horizons, and infer sub-structures (Figure 7). From the lithological cross-section of these wells (Figure 7), trachyte is the dominant rock unit, with intercalations of pyroclastics, tuff and syenite. Post-caldera pyroclastics, tuff and trachytic lavas make up the upper lithological units; the cuttings exhibit a blocky nature; hence, they are the probable cause of losses in this upper zone. At 320 to 400 m, a tuff marker horizon was noted in all the wells, except for well MW-01 where the horizon appeared at 452 to 496 m. The tuff marker horizon was interpreted to be of Syn-caldera age. Another tuff marker horizon was encountered roughly between 450 and 750 m, where normal faults are interpreted between wells MW-01/ MW-06; MW-06/ MW-13; MW-13/ MW-09; MW-09/ MW-12 and MW-12/ MW-04.

Strecker and Melnick (2013) confirmed the presence of numerous linear structures in the central region of Menengai caldera (Figure 3), within which all the mentioned wells are located. Another tuff marker horizon was observed at about 1620 to 1700 m, though is evidently absent in wells MW-09 and MW-12. Finally, a syenitic marker horizon occurs at 1800 m to the bottom in nearly all the wells, with fresh glass being encountered in wells MW-04 and MW-06 at 2082 m and 2174 m, respectively. Perhaps the syenitic intrusion and the fresh glass occurrence are both related to a relatively shallow magma chamber below the Menengai volcano (Leat, 1984).

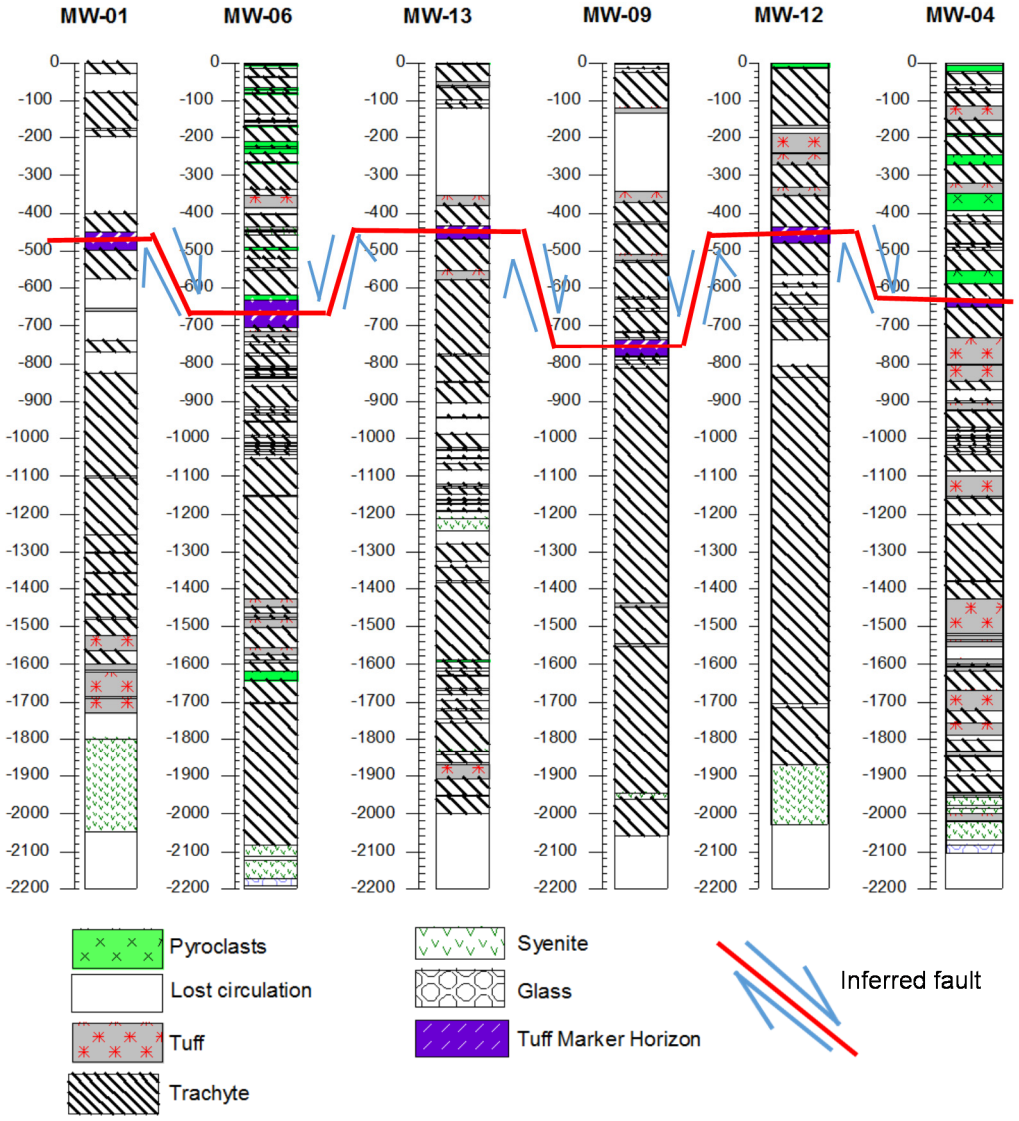

FIGURE 7: Stratigraphic correlation of wells MW-13, MW-01, MW-04, MW-06, MW-09 and MW-12 (GDC, 2013a, Mibei, 2012 and Lopeyek, 2013); inferred fault displacements are shown as half-arrows

An attempt to evaluate the throw, dip and strike of the inferred faults was made and the results are shown in Figure 8. This, of course, is very preliminary as limited data are available, particularly, structural geology. However, the regional NNE-SSW faults (Figure 3) may be cutting across the caldera floor. Furthermore, there are indications that some local faulting is present, for example, the ESE-WNW faulting seen in Figure 3. Figure 8 shows a possible scenario of faulting in the research area. From Figure 7, using the tuff marker horizon, it is inferred that there are faults between several of the Menengai wells. To some point, the throw can be

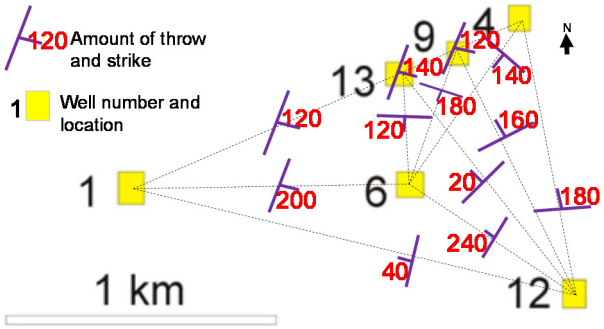

FIGURE 8: Inferred normal faults along wells MW-01, MW-04, MW-06, MW-09, MW-12 and MW-13, showing the inferred strike and throw of possible faults

deduced but it is difficult to define the strike. There seems to be a uniform strike across wells MW-01, MW13, MW-09 and MW-04, as indicated in Figure 8, with a throw averaging 130 m. Correlating the other faults, however, is highly complicated. It is known that the caldera was formed in at least two events, 29 ka and 8 ka ago (Macdonald et al., 2011), which complicates the tectonic scenario. One could also imagine that, in between these events, there might have been stepwise collapses, presently undetected, which could possibly explain the tectonic setting as deduced in Figure 8. It is, therefore, recommended that more detailed structural mapping should be executed to verify the existence of these deduced faults.

5. HYDROTHERMAL ALTERATION

Hydrothermal alteration is, in the simplest terms, a process by which rocks interact with hot fluids and, as such, primary minerals are transformed to secondary ones, with regard to their texture, structures and chemistry. It is fundamental to note that altering of parent rock institutes changes to various physical characteristics of rocks such as porosity and permeability. Reyes (2000) published a simplified and calibrated scale of hydrothermal alteration minerals (Figure 9) which shows the relative temperatures at which the various minerals are stable. Permeability and effective porosity, moreover, are vital to the flow of hot fluids; it is obvious that hydrothermal alteration increases with increased permeability and porosity. These two constraints allow for precipitation of alteration minerals in cavities.

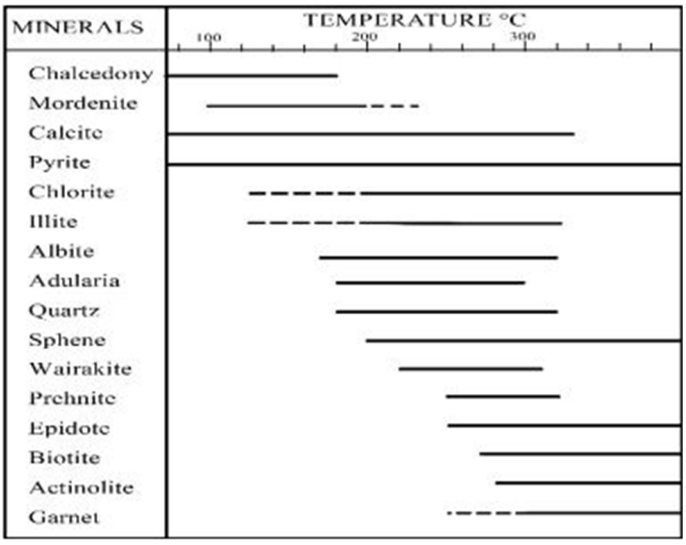

FIGURE 9: Common hydrothermal alteration minerals used as geothermometers and their temperature stability ranges (Reyes, 2000)

5.1 Alteration of primary minerals

As stated previously, trachyte is the dominant rock formation in well MW-13, followed by tuff, syenitic intrusions and minor pyroclastics. Volcanic glass, olivine, feldspar, pyroxenes and opaque minerals are the principal primary minerals observed in this well. When subjected to geothermal environments, the primary minerals are transformed to secondary ones via a number of processes such as replacement, deposition, and so on. The Bowens reaction series (Figure 10) illustrate a relative sequence on how the primary minerals are altered; the first minerals to form are also altered first, and vice versa. A discussion on how primary minerals alter in well MW-13 follows, in a decreasing order of susceptibility to alteration:

Volcanic glass: Even though not a mineral, glass is considered significant because it is very sensitive to alteration, and forms crucial hydrothermal minerals such as zeolites, clays, quartz and calcite, as observed in the study well. Volcanic glass forms from rapidly cooling magma. In well MW-13, volcanic glass, under a binocular microscope, is obsidian-like, black, aphanitic in texture and shows a good conchoidal fracture. In thin section analysis, altered glass is brown and anisotropic. Glass alteration starts right at the top (16 m), and increases to almost 100 % at about 100 m.

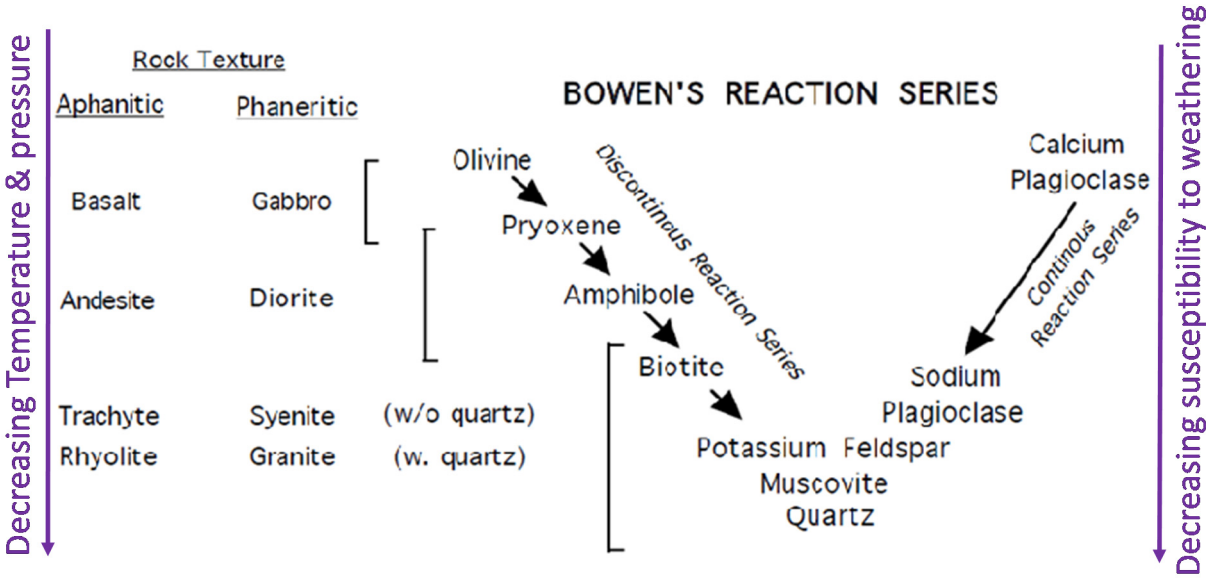

FIGURE 10: The Bowens reaction series (modified from Njue, 2010)

Olivine: In well MW-13, olivine is scarce and rarely fresh. It is distinguished by its unique irregular, sub-angular shape, as well as irregular fractures on the surfaces, often filled with altered minerals. In petrographic analysis, olivine is seen to not have clear cleavage, has parallel extinction and is easily distinguishable from pyroxenes, especially by its low relief and high birefringence. Olivine in well MW-13 is altered to clays and/or replaced by calcite. Its alteration is observed to set in at a depth of 88 m and, at 600 m, olivine is fully altered.

Feldspars: Feldspars form the most dominant mineral in well MW-13, especially in trachyte and in syenitic intrusions, noted by the felsic nature in these rock units. The principal feldspars encountered in this well are sanidine and plagioclase, both appearing in the groundmass and as phenocrysts. In cuttings, feldspars are observed as elongated, transparent to white/grey translucent crystals, occasionally showing twinning. They are distinguished from pyroxenes, quartz and zeolites by their simple twinning, low relief and non-pleochroism. Albite-alteration, noted by its dirty-like appearance and absence of twinning, first appears at 606 m in well MW-13. At the same depth, feldspars are noted to alter into clays and are also replaced by calcite, all the way to the bottom of the well. At 1220-1500 m, feldspar alteration increases to nearly 70%; epidote and quartz are observed to form from feldspars at this depth range.

Pyroxene: Pyroxenes are one of the earliest rock forming minerals and are resistant to alteration. In thin sections, they are easily identifiable by their good cleavage, moderate relief and interference colours, and straight extinction (orthopyroxene) or inclined extinction (clinopyroxene). In well MW-13, pyroxenes are observed as pale green to pale brown, with a metallic lustre and stubbier crystals, either embedded in a feldspar-rich groundmass or as phenocrysts. Alteration of pyroxene to clays and calcite was first noted at 830 m and 1174 m depth, respectively. The alteration increases to about 50%, starting from 1500 m to the bottom, the minerals being altered to calcite, actinolite and high-temperature clays.

Opaque minerals: These minerals are mainly marked by Fe-Ti oxides, and are quite resistant to alteration. In petrographic studies, fresh opaque minerals do not transmit light, and when altered, they allow light through and have an extremely high refractive index. Opaque minerals in well MW-13 alter into sphene and pyrite. Sphene was first noted at 606 m, and continues to the bottom of the well.

5.2 Description and distribution of hydrothermal alteration minerals in well MW-13

Several alteration minerals are observed in well MW-13 and their distribution is shown in Figure 11. Below is a description of the hydrothermal alteration minerals encountered in the studied well (in the order of increasing temperature).

Amorphous silica and chalcedony are the first alteration minerals observed in well MW-13. In the cuttings, the two almost similar minerals appear as vesicle and cavity in-fills (as coating along the walls) from 20 to 62 m depth. Chalcedony is pale blue, purplish to milky white in colour and appears as a lining of roundish crystals, while amorphous silica exhibits more or less the same colours but without a clear crystal form. At greater depths, chalcedony is replaced by secondary quartz.

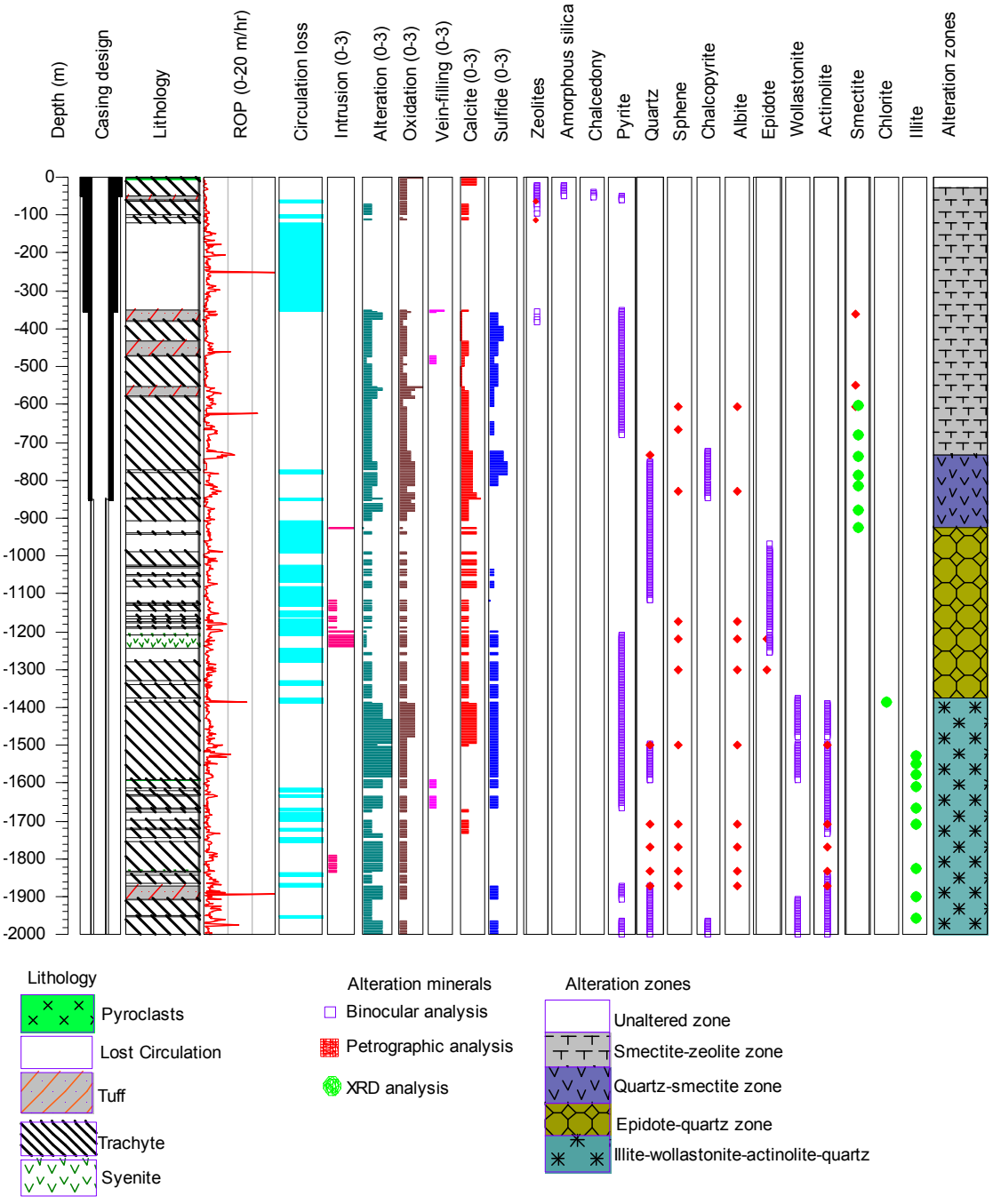

FIGURE 11: Distribution of hydrothermal alteration minerals in well MW-13

Zeolites mainly occur in fractures and vesicles and are milky white to transparent. In thin sections, zeolites are distinguished from quartz by their lower refractive index and obvious radiating and fibrous nature. According to Saemundsson and Gunnlaugsson (2014), zeolites are formed at relatively low temperatures (of up to 130°C) and are rarely associated with very intense alteration. They are found as minor constituents in altered rocks, and are sometimes formed from re-crystallization of volcanic glass (Kristmannsdóttir and Tómasson, 1978). Thomsonite and scolecite were first noted for sure at 26 m and 112 m, respectively. The zeolites then occur intermittently, in a minor amount, down to 382 m depth.

Secondary quartz appears as colourless to white hexagonal, euhedral to subhedral crystals, filling the cavities. In the cuttings, quartz is differentiated from zeolites by its higher refractive index. Secondary quartz is first seen at 750-1188, 1496-1592 and 1872-2000 m.

Calcite is easily distinguishable from feldspars by its high interference colours, fairly high relief and its obvious cleavage. In binocular analysis, calcite is best identified using dilute hydrochloric acid. This mineral is related to boiling, dilution and condensation of carbon dioxide in a geothermal system (Njue, 2010). It is worth noting that calcite may be formed by heating up fresh groundwater and, hence, is not related to geothermal activity all the time. This explains the reason for the appearance of calcite in nearly the entire well column. Abundant calcite was noted at 834-850, 926-1118 and 1390-1496 m.

Sulphides are ore minerals, primarily composed of metal and sulphur, and are commonly associated with intrusive activity in Iceland (Saemundsson and Gunnlaugsson, 2014; Holwell et al., 2012). Studies on sulphide ores led to the discovery of hydrothermal systems in the deep oceans (Vaughan, 2006) which further confirms that the presence of these minerals designates high permeability. In well MW-13, sulphides occur as disseminations, blebs and massive aggregates on the surfaces of cuttings, or are deposited in the cavities. *Pyrite* and *chalcopyrite* were positively identified in well MW-13. When unaltered, the two minerals exhibit a brassy yellow metallic lustre, with chalcopyrite having a distinct iridescent tarnish. Pyrite was first seen at 50 to 62 m in a tuff formation, deposited in the vesicles. It reappeared at 358 m, and continued irregularly to the bottom. Chalcopyrite first appeared at 722 to 750 m. The mineral only appeared again at the bottom-most section of the well.

Albite occurs as an alteration product of plagioclase feldspar. The mineral is distinguishable by its lower refractive index, lack of clear twinning, as well as its somewhat dirty appearance. Fractures on primary plagioclase minerals mark the first indication of alteration. Albite in well MW-13 was first observed at 606 m and extends to the bottom of the well.

Sphene forms at nearly all temperatures. It is opaque but transmits light when broken down to form titanite, and exhibits an extremely high refractive index. Sphene, in thin section, appears brown in colour with a very high relief and occurs as uneven sub-angular grains replacing opaque minerals. The mineral was first sited at a shallow depth of 606 m and remained sporadically to the bottom.

Epidote is distinguishable by its characteristic yellow green colour, both in binocular and petrographic analysis. Its appearance indicates a representative alteration temperature of about 240°C. Epidote was first observed in well MW-13 at 982 m as a yellow green transparent non crystalline mineral disseminated on the surfaces of cuttings. At 1508 m, epidote was evidently observed as prismatic crystals in a vesicle. Epidote at this depth occurs in association with quartz, pyrite and wollastonite.

Wollastonite gives a representative temperature of 270°C and remains stable even at temperatures beyond 300°C. It is easily identifiable in cuttings by its woollen-white-hair-like crystals that are commonly very fragile and fibrous. In petrographic analysis, this mineral is transparent and non-pleochroic. Wollastonite is known to occur in association with garnet and epidote in high-temperature systems (Saemundsson and Gunnlaugsson, 2014**)**; it occurred with epidote, quartz, pyrite and actinolite in well MW-13. Wollastonite's first appearance was at 1376 m, and continued sporadically to the bottom of the well.

Actinolite may be confused for wollastonite because it is also fibrous but exhibits a slightly greenish colour, and is rarely deposited in vesicles. Actinolite occurs in very dense slender thread-like crystals embedded in the groundmass, and occurs mainly adjacent to intrusive bodies or deep in high-temperature geothermal systems. The mineral forms at a higher temperature of more than 280°C. In well MW-13, actinolite was first sited at 1388 m, and conspicuously continued, at alternating lithology sections, to the well bottom. At 1502 to 1590 m depth, the occurrence of actinolite was noted to be more abundant; this zone is relatively more altered and is interpreted to be a feeder zone, as will be discussed later.

Clays are common alteration products of nearly all rock-forming minerals and thus they appear from top to bottom of the well column. Clay minerals are phyllosilicates that bear water, trapped between their silicate sheets in large quantities. The minerals have different capacities of holding and/or releasing water, which contributes to variations in the clays; crystallinity changes with temperature. Typically, clay minerals form microscopic to sub-microscopic crystals (in some cases, crystallinity is totally limited); hence, it becomes a bit complicated to study these minerals under a microscope. As a result, and in order to compliment petrographic and binocular analysis, X-ray diffraction analysis for 36 samples in well MW-13 was carried out. Three types of clays were positively identified, as discussed below:

Smectite is a low-temperature (> 200°C) clay, easily distinguishable by its fine-grained brown texture and low birefringence in thin sections. The clay shows a swelling characteristic feature; therefore, smectite exhibits a variety of peaks in the XRD analysis. In well MW-13, smectite was first positively identified at 362 m in thin sections, and at 604 m in the XRD analysis. The recorded peaks were from 12.8 to 15 Å when untreated, 12.9 to 15.8 Å when treated with glycol and collapsing to 10.3 Å when heated (Figure 1 in Appendix I).

Chlorite is well distinguishable in the cuttings by its green radiating and fibrous crystals, mainly occurring in the vesicles. In the thin sections, chlorite is green in open polars and turns grey in crossed view. It is also weakly to non-pleochroic, and shows low birefringence. In the study well, chlorite first appears at 1384 m and was not present in subsequent samples. It exhibits characteristic unchanged peaks of 14.50 and 7.28 Å when untreated and glycolated, and completely collapses after being heated to 550°C. It signifies a minimum temperature of 200°C (Reyes, 2000).

Illite occurrence indicates temperatures greater than 200°C. The clay forms when K-feldspars are replaced and was first observed in the XRD analysis at 1526 m. In well MW-13, illite was not identifiable in either binocular or petrographic analysis; but in the XRD analysis, its characteristic 10.3 Å peak did not change in the untreated, glycolated and heated conditions (Figure 3 in Appendix 1).

5.3 Vesicles and vein fillings in well MW-13

Vesicles are open cavities in rocks that form when dissolved gases in molten magma escape during crystallization, when magma is erupted; the empty pores may later be filled by secondary minerals to form an amygdaloidal texture. On the other hand, veins are irregular discontinuous dike-like fissures/fractures in rocks that may be filled with secondary minerals and/or fluids. Veins and vesicles are important geothermal structures because they are good sources of permeability and porosity. Additionally, they allow the deposition of secondary hydrothermal alteration minerals which helps in estimating reservoir temperatures. Furthermore, the time sequence in which alteration minerals deposit in voids and fractures informs on the evolution of a geothermal system (Franzson, 2014), and reports on changes in the geothermal system with time. Proper studies on the deposited minerals give a very useful picture on the present conditions in a geothermal system, i.e. whether it is cooling, heating or in equilibrium.

Exclusive use of rotary bits may unfortunately cause loss of the important aforementioned textural relationships (Lagat, 2004). This seems to have affected cuttings from well MW-13. Nevertheless, a few amygdales were noted; their sequence will be discussed later. In the 20 topmost sections, the vesicles were notably void. Low-temperature minerals such as zeolites, chalcedony, pyrite, calcite, quartz and clays were observed in voids from 20 to about 400 m. Zeolites and chalcedony evidently disappeared earlier while the rest carried on to greater depths. At 1200 m to the bottom, high-temperature mineralisation characterizes the vesicles and veins, for instance, wollastonite, epidote, actinolite and clays.

5.4 Mineralogical evolution in well MW-13

The time sequence, during which secondary minerals form in voids, gives a clear picture on the evolution of a geothermal system. The mineral deposition sequence informs on the history of a geothermal system, as well as predicting its future (Njue, 2010). Moreover, different minerals are stable at different physical and chemical conditions such as temperature, as previously discussed. Study of the order at which the minerals form can, therefore, act as a guide on the reservoir status of a system at the present time and, preferably, on the past and future as well. Only two paragenetic sequences (in vesicles) were clearly observed in well MW-13, demonstrated in Table 1, based on petrographic analysis.

TABLE 1: Mineral depositional sequence in well MW-13

Depth (m)	Alteration Sequence Early……...Late
1220	Calcite-albite-epidote
1500	Calcite-actinolite-chlorite

5.5 Mineral alteration zones

Based on the formerly mentioned different analyses, four different mineral alteration zones were recognized in well MW-13 (Figure 11). The zones are comprised of:

Unaltered zone (0-30 m): Lithologically, the zone is characterized by fresh pyroclastic and trachytic formations. Only surface alteration (oxidation) is notable in the cuttings.

Smectite-zeolite zone (30-750 m): This zone is marked by the intermittent presence of zeolites (thomsonite and scolecite) as well as smectite clays. Other alteration minerals in this zone include chalcedony, calcite, and pyrite. This mineralogical assemblage indicates temperatures below 200°C, inferred from the low-temperature minerals. The zone is also characterized by tuff and trachytic rock units, with sporadic circulation losses.

Quartz-smectite zone (750-982 m): The zone is marked by the first appearance of secondary quartz at 750 m. An increase in oxidation is notable in this zone (Figure 11). Trachyte and minor circulation losses characterize the zone, too.

Epidote-quartz- zone (982-1376 m): This zone is marked by the first appearance of epidote at 982 m. Additional alteration is noted by the occurrence of calcite, sulphides (e.g. pyrite), albite and oxidation. The mineralogical assemblage of this zone indicates temperatures above 200°C. The zone is mainly composed of blocky trachyte.

Illite-wollastonite-actinolite-quartz zone (1376-2000 m): This is the last mineralogical assemblage marked by high-temperature wollastonite and actinolite minerals, observed first at 1376 m and 1388 m, respectively. Temperatures in this zone exceed 270-290°C. Quartz remained persistent in this zone, as well as sporadic appearance of calcite, pyrite, albite and oxidation.

5.6 Fluid inclusion geothermometry

Alteration temperatures and temperatures logged soon after drilling is completed may not be reliable in defining the formation temperature of a geothermal system. Consequently, there is a definite need to compliment the various analyses, as discussed earlier. Fluid inclusion geothermometry, also termed microthermometry, involves investigating various phase variations in fluid inclusions under controlled conditions of heating and cooling (Harvey and Browne, 2000). Primary inclusions are trapped during the growth of crystal while secondary ones are formed during the healing process of a crystal.

In well MW-13, a total of 71 fluid inclusions, trapped in two grains of secondary quartz at 1550 m depth, were analysed. The comparative results are presented on a histogram (Figure 12). Based on measured and hydrothermal alteration temperatures, this zone has estimated temperatures ranging as high as 240 to above 300ºC. GDC (2013b) reports a feed zone at 1500-1650 m depth range. The homogenization temperatures were measured in regular intervals, ranging between 275 and 320°C. Though not very clear, there seem to be two populations of the recorded temperatures. The lower temperature range is from 275 to 295°C, and the higher temperature range roughly records 300 to 315°C.

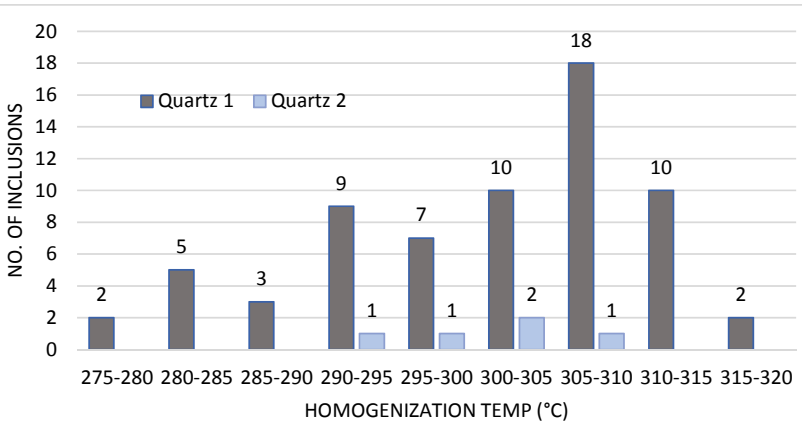

FIGURE 12: Histogram showing the results of fluid inclusion analysis in well MW-13

6. AQUIFERS

A geothermal aquifer is an underground permeable layer of rock or unconsolidated materials (gravel, sand, or silt) bearing hot fluids, including gases, which are extracted for geothermal exploitation. Aquifers, or feed zones, are located using various data such as temperature logs, circulation losses, well completion tests, hydrothermal alteration, and so on. Drilling parameters such as penetration rates (ROP) are also very useful; for instance, a high ROP may indicate the presence of an aquifer. Temperature logs indicate the location of both inflow and outflow in a well, whether cold or hot. Similarly, high hydrothermal mineral alteration is deduced to indicate permeability. Permeability enhances the flow of fluids, consequently leading to increased rock interaction with the geothermal fluids which may lead to a sudden increase in alteration minerals. Circulation losses may also indicate permeability, though care must be taken when using this parameter; other technical measures may cause the losses, for example, cuttings may get stuck in other fractures deep down the wellbore. It is worth noting that aerated drilling may cause slight disturbances in air/water equilibrium, thus causing circulation losses that are not necessarily related to feed zones.

In well MW-13, the first measured temperature log (3 hours heating in Figure 13) evidently showed an obstruction at approximately 1050 m. Therefore, pumping was conducted as an intervention measure. The second temperature log (15 minutes heating) showed higher temperatures at the inferred permeable 1400 to 1600 m section of the well, while the subsequent two logs indicated lower temperatures, attributed to the inflow of colder circulation fluids. The flowing profile confirms a progressive recovery of well temperature, but the profile also indicates stagnant conditions in the well from 1500 m to the bottom.

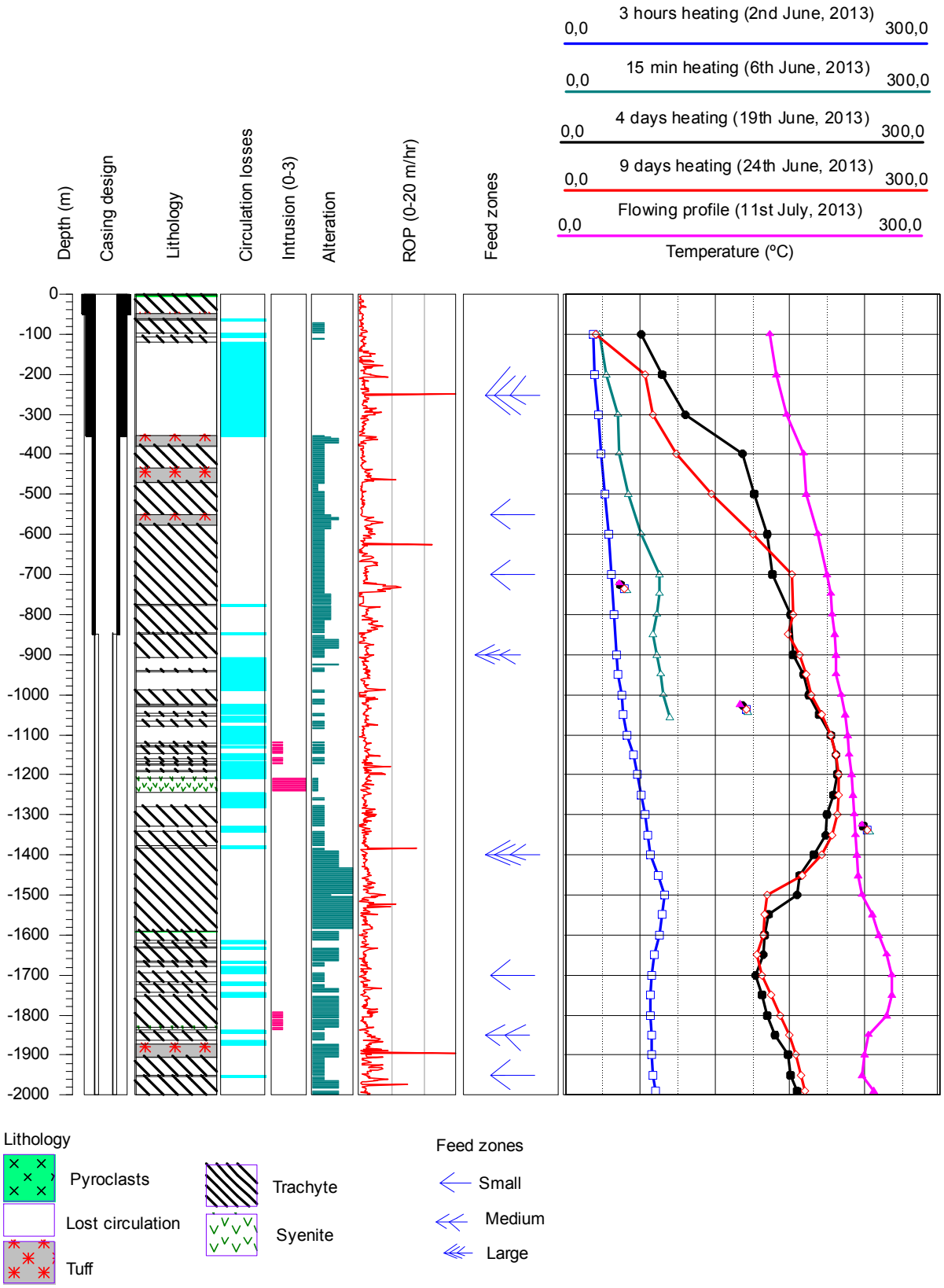

FIGURE 13: Well MW-13 aquifers deduced from the correlation of temperature logs, rates of penetration and lithology characteristics

6.1 High permeability zones

Having studied the stratigraphy, hydrothermal alteration and different temperature profiles, it becomes easier to deduce the location of feed zones in well MW-13. Temperature logs, circulation losses, increased alteration, penetration rates and lithological characteristics have been correlatively used to infer eight permeable zones in the study well. The feed zones are classified as either small, medium or large (Figure 13).

120-352 m is a large permeable zone, probably with several feed points, and was identified above the production portion of the well. The zone is inferred to be cold, hence it was cased off. The permeable zone was deduced from circulation losses and an increased rate of penetration during drilling.

550 m is a small feed zone associated with a tuff formation. It also appeared above the production section and was cased off. It was deduced from increased penetration rates, alteration and temperature.

700 m is associated with a fractured trachyte formation, as indicated by the increased ROP and circulation losses. A temperature gain was also notable at this zone which is above the production area.

900 m is the first large aquifer encountered within the production portion of the well. The aquifer is associated with a rise in temperature, as indicated by the 4 day duration heating log, circulation losses, and increased ROP. A slight increase of hydrothermal alteration was also notable.

1500 m is believed to be the depth of the main feed zone in well MW-13, where temperatures indicated a rise to more than 240°C during the flowing profile (Figure 13). The zone is characterized by high-temperature hydrothermal minerals, as previously shown in Figure 11, as well as circulation losses and increased penetration rates. At this zone, the earlier temperature logs (conducted shortly after pumping due to an obstruction) indicated a sharp decrease in temperature while a later profile (flowing) showed a rise at the same section. This indicates a colder inflow during pumping into the permeable zone, with a later remarkable recovery.

1700 m is a small hot feed zone marked by circulation losses, increased alteration and a temperature rise. For instance, the 4 day heating log showed a rise in temperature at 1700 m.

1850 m is linked to a permeable tuff formation, as indicated by increased penetration rates as well as circulation losses. The medium size aquifer was also deduced from increased alteration and temperatures (at 1850 m, a temperature increase was noted from the 4 day heating up profile).

1950 m is inferred to be responsible for the temperature rise at the well's bottom. The small feed zone is also associated with increased penetration rates and circulation losses.

6.2 Correlation of measured, formation, alteration and fluid inclusion homogenization temperatures

Formation and measured temperatures in a well may differ for a number of reasons. For instance, circulation during drilling cools the well. Given ample time, the well temperatures will recover and eventually equilibrate with the formation. It may also remain uncertain whether the observed alteration minerals reflect the current conditions in the geothermal system, or if they are related to different past thermal events (Lagat, 2004). Fluid inclusion homogenization temperatures are most reliable in interpreting temperatures of past geologic events (Sorby, 1858 in Roedder, 1984). However, microthermometry is time consuming and it is not logical to conduct the analysis for the entire well column. Besides, inclusions may not be always present. However, despite all such reservations, it is important to correlate all the temperatures with the aim of understanding the geothermal system in a deeper perspective.

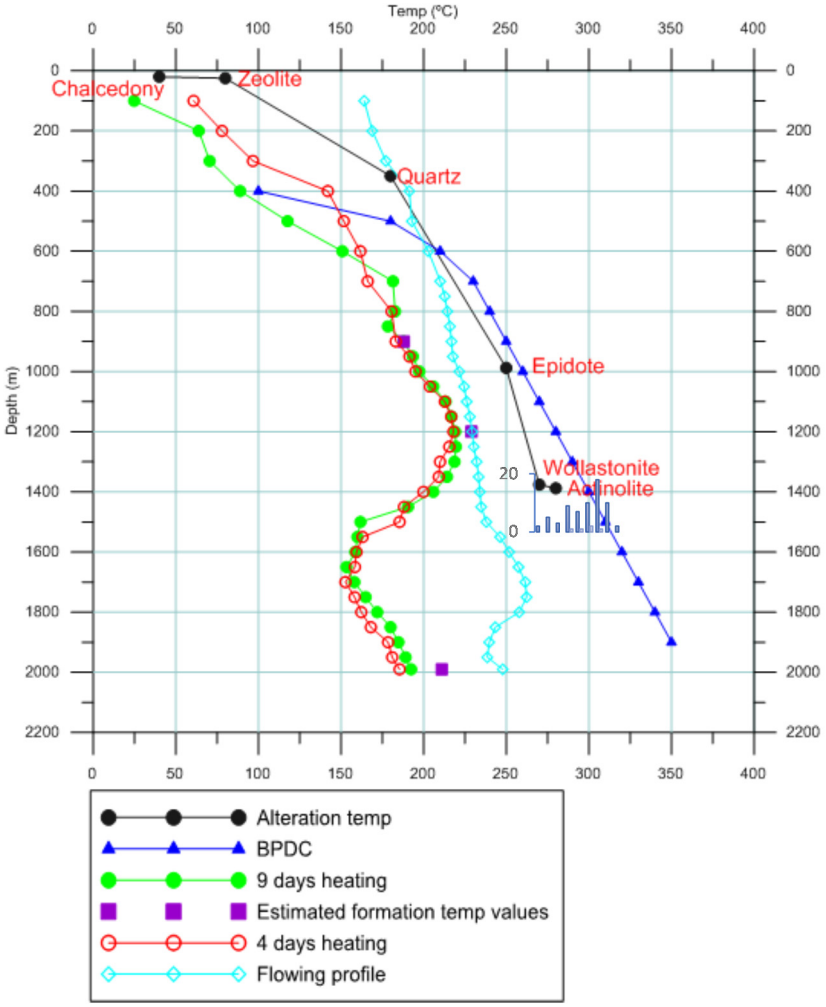

FIGURE 14: Correlation of measured, formation, interpreted hydrothermal alteration and fluid inclusion temperatures in well MW-13

Figure 14 demonstrates the correlation of measured, -formation, -alteration and fluid inclusion temperatures in well MW-13. The formation temperature was inferred from the measured temperatures, using Horner's method. However, it should be noted that the inference is not sufficiently reliable, as the 9 day heating time period (Figure 13) may not have been long enough for the well to have heated up sufficiently. The interpretations made are based on the assumption that the inferred formation temperature represents current conditions in the system.

On correlating fluid inclusions geothermometry with formation temperature, a progressive heating is notable; the recorded quartz homogenization temperature (298°C on average) is higher than the current formation temperature. The interpreted hydrothermal alteration temperature is in equilibrium with the fluid inclusion measurements and plot along or close to the boiling point curve. This indicates that at some point, the system experienced boiling conditions. On the other hand, when the measured temperature is compared with homogenization, formation and interpreted alteration temperatures, a significant difference is seen. This, as explained earlier, is deduced to be attributed to pumping, due to a previous obstruction.

7. CLAY ALTERATION IN OLKARIA VOLCANIC COMPLEX

7.1 General information

The Olkaria volcanic complex is a Quaternary volcanic system located within the Kenyan rift system, south of Lake Naivasha (Figure 1). Macdonald et al. (2008) described the complex as a relatively young (20 ka), small-volume system dominated by frequent formations of peralkaline rhyolitic domes. Geothermal exploration and development have been ongoing in this high-temperature geothermal field since the early 1970s. Omenda (1998) reported the age of the rocks in the Olkaria complex to range from Pliocene to Holocene (4.5 to 0.4 Ma). The geology consists of four major formations, namely: the Upper Olkaria volcanics, Olkaria basalts, Plateau trachytes and Mau tuffs, as classified by Omenda (1998). Simiyu (1999) proposed the existence of a heat source beneath the complex, at about 6 km depth.

The fluid chemistry of this system is controlled by sodium bicarbonate and sodium chloride waters (Malimo, 2009) with calcite occurring as the most abundant carbonate (Omenda, 1998). The main structures that control permeability in the Olkaria volcanic complex are the N-S, NW-SE, NNW-SSE, and ENE-WSW faults, characterized by high fumarolic activity along the fault lines. The main hydrothermal minerals in the volcanic complex include zeolites, pyrite, calcite, albite, chlorite, epidote, prehnite, quartz, and sphene (Lagat, 2004; Ronoh, 2012).

7.2 Classification and occurrence of clays in Olkaria field

The distribution of clay minerals within a geothermal system gives important insights on the hydrology of the system. Additionally, clays are temperature dependent minerals and are, therefore, useful in predicting temperatures in the geothermal reservoir. The occurrence of low to high- temperature clays in Olkaria geothermal field (Figure 15) was confirmed during the exploratory drilling phase by Leach and Muchemi (1987). Additionally, numerous studies have been published on hydrothermal alteration in the Olkaria geothermal wells (Omenda, 1998; Lagat, 2004; Ronoh, 2012, Okoo, 2013). More specifically, the geothermal field is characterized by four types of clays which are noted mostly as vein and vesicle fillings. The clays include *smectite, kaolinite, illite* and *chlorite*, as seen in wells OW-902, OW-903, OW-39A and OW-912B, based on petrographic and XRD analyses.

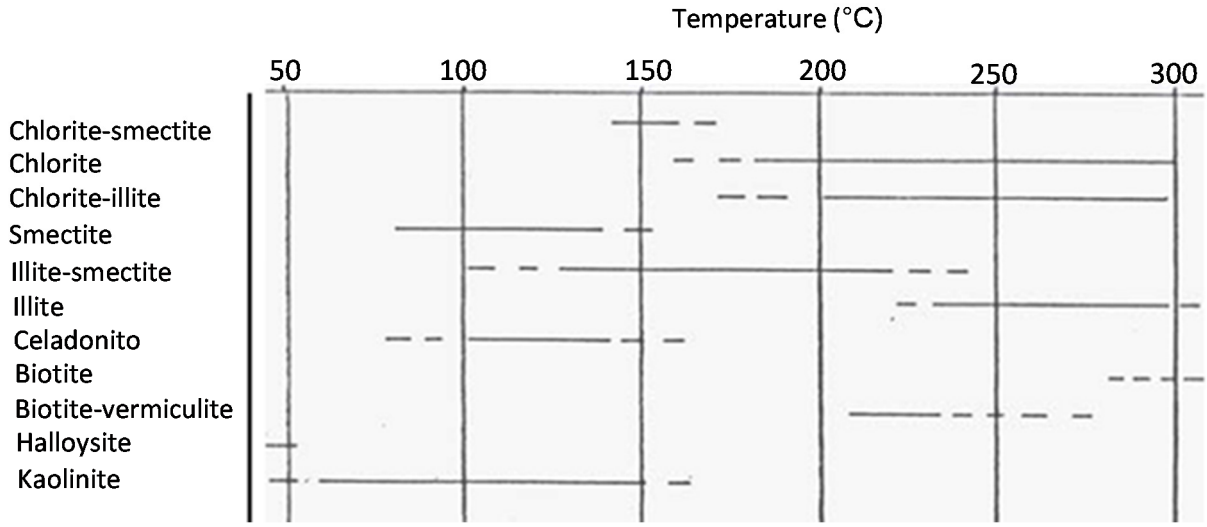

FIGURE 15: Clay minerals and their temperature ranges in Olkaria exploration wells (adapted from Leach and Muchemi, 1987)

7.3 Clays in Menengai field versus Olkaria field

Based on clay analysis results for Menengai wells, e.g. MW-13, MW-11, MW-06 and MW-08 (Mibei, 2012; Kipchmba, 2013), smectite clays are present at shallow depths (Figure 16) whereas, at present, smectite has not been detected, except in small amounts by XRD in Olkaria (Lagat, 2004; Musonye, 2012; Njathi, 2012; Ronoh, 2012; Mwangi, 2012; Otieno and Kubai, 2013; Okoo, 2013). However, in Olkaria wells, for example in wells OW-902, OW-903, OW-39A and OW-912B, illite and chlorite, high-temperature clays, first appear at shallower depths than observed in Menengai (Figure 16). It is striking, therefore, that high-temperature clays appear earlier in Olkaria than in Menengai. It has been speculated that the dissimilarities in the occurrence of clays in Menengai and Olkaria fields is due to age differences between the two systems. The Olkaria system is probably older and, therefore, the geothermal system may have had a longer time to evolve, as opposed to the Menengai system. Of course, other factors such as differences in the permeability of the two fields cannot be ruled out without sufficient evaluation.

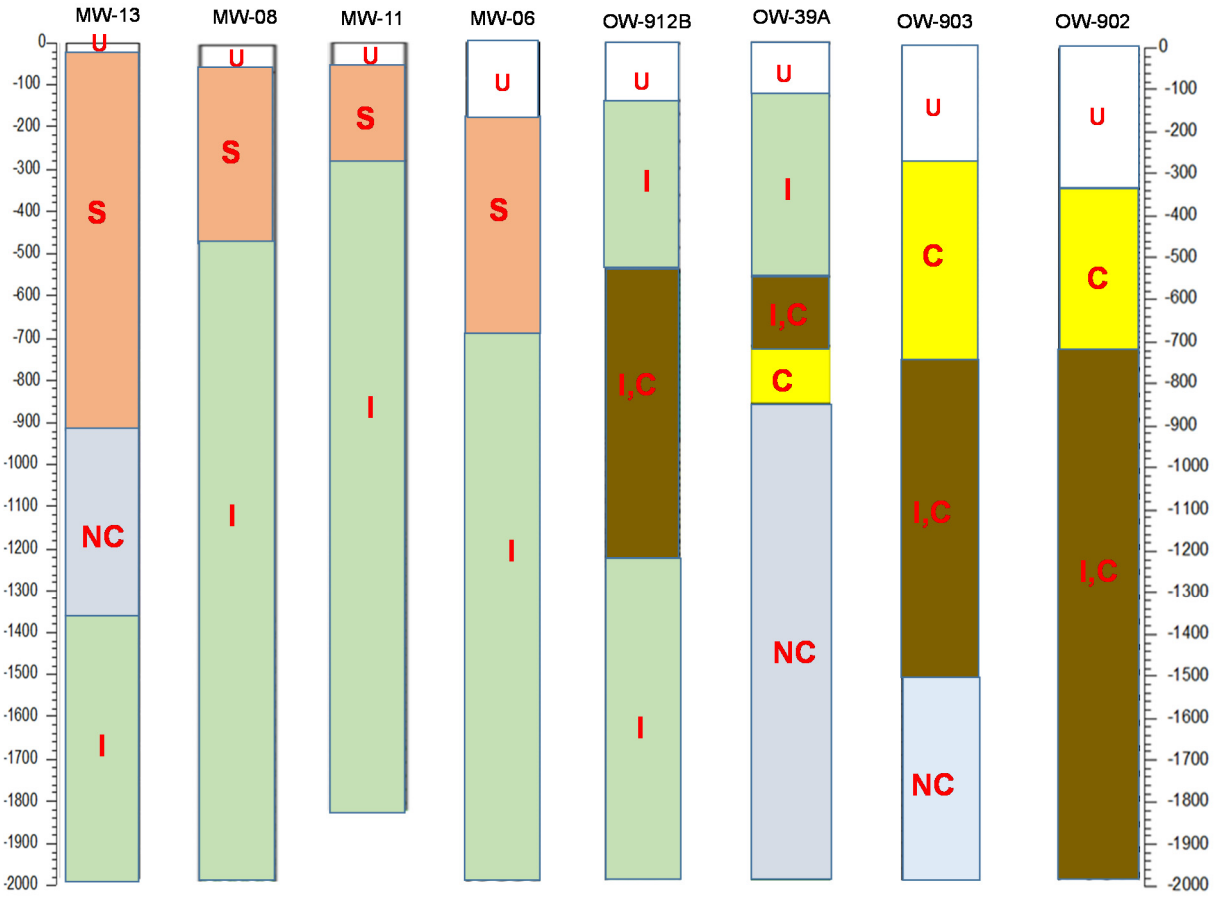

FIGURE 16: Clay occurrence in Menengai versus Olkaria wells; NC = no identifiable clays, U = unaltered, S = smectite, C = chlorite, I = illite (modified from Mibei 2012; Kipchumba, 2013, Lagat, 2004; Okoo, 2013; Ronoh, 2012)

8. DISCUSSION

The litho-stratigraphy of well MW-13 closely correlates to that of most other wells previously drilled in Menengai geothermal field, i.e. MW-01, MW-04, MW-06, MW-09 and MW-12, as demonstrated in Figure 8. Trachyte, tuff, pyroclastics and syenite are the four rock units encountered in well MW-13, with trachyte being the most dominant. The upper 300 m is characterized by pyroclastic and trachytic lavas of Post-caldera age, inferred from their heterogeneous and blocky nature (Leat, 1984), well-demonstrated in the cuttings. In well MW-13, a brownish to greenish tuff formation encountered from 434 to 472 m is deduced to correlate to a Syn-caldera marker horizon, separating the Post and Pre-caldera lavas in Menengai caldera. From 472 m to the well bottom, the lithology is characterized by Pre-caldera lavas, mainly trachytic, intercalated by thin lenses of tuff and syenitic intrusion.

Stratigraphic correlation of well MW-13 and other studied wells within the caldera reveals several normal faults (Figure 7), inferred from the Syn-caldera tuff marker horizon. Only a few of the faults seem to display a consistent throw and strike (Figure 8). The tectonic scenario may be significantly complicated as a result of the two caldera-forming events, 29 ka and 8 ka, respectively (Macdonald et al., 2011). Additionally, the two collapse events might have taken place in a stepwise manner, presently undetected, which could possibly explain the tectonic setting as deduced in Figure 8. It is, therefore, recommended that more detailed structural mapping should be executed to verify the existence of these deduced faults.

Litho-stratigraphic correlation displays a fairly similar sequence in the evolution of the Menengai volcano. For instance, the youngest lavas appear on the uppermost part of the litho-stratigraphy. The different textures in the cuttings further confirm the different eruption episodes of the volcano. A pyroclastic formation at approximately 1600 m is noted in wells MW-06 and MW-13; the deeper sequence signifies an old land surface, appearing as a reddened oxidized soil horizon. Additionally, a syenitic intrusion characteristically appears at the bottommost part. It probably relates to the proposed existence of an axial intrusion beneath Menengai volcano (Leat, 1984).

Hydrothermal alteration minerals in well MW-13 were observed deposited in vesicles, cavities and veins and/or as replacements of primary minerals. Different alteration minerals are stable at different physico-chemical conditions, e.g. temperature (Reyes, 2000). The minerals can, therefore, be used to accurately predict the alteration temperatures in a system. In well MW-13, low-temperature minerals, such as zeolites, characterized the upper sections. The system gradually evolved to form high-temperature minerals such as epidote, wollastonite and actinolite, occurring at 982 m, 1376 m and 1388 m, respectively. Additionally, some alteration minerals, such as sulphides, are directly related to permeability. In the study well, pyrite and chalcopyrite appear in significant amounts where the formation is believed to be permeable. The occurrence evidently decreases towards the well bottom (Figure 11), probably indicating reduced effective permeability. Besides, the time sequence in which alteration minerals deposit, informs on the evolution of the geothermal system. From the study, four mineral alteration zones have been identified. In order of increasing depth, the mineralogical assemblages include (1) the smectite-zeolite zone, (2) the quartz-smectite zone, (3) the epidote-quartz-zone, and (3) the illite -wollastonite-actinolite-quartz zone.

The homogenization temperatures (Th), recorded in 71 fluid inclusions from two quartz crystals at 1550 m, range from 275 to 320°C. The average 298°C homogenization temperature is higher than the current formation temperature, thus, progressive heating is notable. The inferred hydrothermal alteration temperature is in equilibrium with Th, and both plot along or close to the boiling point curve. This indicates that the system experienced boiling conditions at some point in its life. Since then, slight cooling might have occurred. The comparison of the measured temperature with the other types of temperatures shows a significant difference. This is attributed to the vast volume of cold water that was pumped into the well during drilling operations. When drilling is completed, this water flows back into the well. It is clear that the well had not yet recovered to formation temperatures when the heating-up temperature logs were executed. It is worth noting that the flow profile shows a positive temperature recovery at shallower depths but, from 1500 m, the profile shows stagnancy in the flow which probably indicates reduced permeability.

Eight permeable zones were inferred from a correlative analysis of temperature logs, circulation losses, increased alteration, formation penetration rates and lithological characteristics. However, critical caution should be emphasized when using circulation losses to infer permeability; other technical measures may cause the losses, for example, cuttings may get stuck in other fractures deep down the wellbore, and later on flushed out suddenly. During aerated drilling, slight disturbances in the air/water equilibrium may appear as a circulation loss even though it is not. The temperature measurements for well MW-13 appear insufficient to aid in finding the exact location of the feed points. Nevertheless, ample correlation of the aforementioned parameters has aided in the location of permeable zones at around 120-352, 550, 700, 900, 1400-1600, 1700, 1850 and 1950 m depth. The main feed zones in the well are believed to be at 1400 to 1600 m. From the flow profile measurements, a rise in temperature to more than 240°C is notable at 1500 to 1850 m (Figure 13). More temperature measurements would be very useful in studying the permeability in well MW-13, which, in turn, would aid in updating the geothermal conceptual model for Menengai field.

An attempt to compare Menengai and Olkaria volcanic systems showed that the two systems closely correlate in terms of geology and geophysics. However, the Olkaria system is 20 ka (Macdonald et al., 2008) and is rhyolite-dominated. On the other hand, the Menengai volcano is trachytic, and is marked by two caldera-forming events, occurring 29 ka and 8 ka ago, respectively (Leat et al., 1984; Leat, 1991;

Macdonald et al., 2011). Thus, it becomes critical to evaluate which system is younger/older. Heat sources are present at about 6 km in both systems (Simiyu, 1999; Simiyu and Keller, 1997; Wamalwa, 2011). Interestingly, high-temperature clays (illite and chlorite) appear in Olkaria wells, for example in wells OW-902, OW-903, OW-39A and OW-912B, at significantly shallower depths than that observed in Menengai in wells MW-13, MW-06, MW-08 and MW-11, as illustrated in Figure 16. Therefore, the other critical question is whether the different ages of the two geothermal systems is responsible for the variations noted in the clay alteration mineralogy. Other probable reasons may be differences in the permeability of the two fields.

9. CONCLUSIONS

The following conclusions can be drawn from the comprehensive study of well MW-13 samples:

1) The lithology is composed of four different rock units, namely trachyte, tuff, pyroclastics and syenite; trachyte is the most dominant. The lithology closely relates to that of previously studied wells. A tuff marker horizon was encountered at around 450 m;
2) The shallow section of the well is characterized by low-temperature hydrothermal alteration minerals which evolved to form high-temperature ones at greater depths. The occurrence of sulphides in the well signifies permeability;
3) Four alteration zones, based on mineralogical assemblages, were identified. They include (1) the smectite-zeolite zone, (2) the quartz-smectite zone, (3) the epidote-quartz-zone, and (3) the illite -wollastonite-actinolite-quartz zone. The uppermost 30 m section is unaltered;
4) The inferred alteration temperature and homogenization temperature plot along the boiling point curve. The system was in boiling conditions at some point in time, and slight cooling may have occurred. The measured temperatures do not reflect the current formation temperature;
5) Eight permeable zones have been identified; the main feed zone is at 1400 m. The feed zones include 120-352, 550, 700, 900, 1400-1600, 1700, 1850 and 1950 m. The main sources of permeability are faults and lithological contacts; and
6) High-temperature clays first appear at shallower depths in Olkaria wells than in Menengai wells. It is highly suspected that the different ages of the two systems are accountable for the differences noted.

ACKNOWLEDGEMENTS

I am genuinely grateful to UNU-GTP and the Government of Iceland for giving me a chance to attend this noble course and for financing it. My very heart-felt appreciation goes to the UNU Geothermal Training Programme staff, Mr. Lúdvík S. Georgsson, Mr. Ingimar Gudni Haraldsson, Ms. Málfrídur Ómarsdóttir, Ms. Maria S. Gudjónsdóttir, Mr. Markús A.G. Wilde, Ms. Thórhildur Ísberg and Rósa for their commitment and unquestionable support till the end of this project work; I have learned so much from your high-level spirit of teamwork and excellence.

To my advisors, Dr. Björn S. Hardarson, Dr. Hjalti Franzson, Ms. Helga Margrét Helgadóttir, Ms. Sveinborg Hlíf Gunnarsdóttir, and Saeunn, Sigurdur, Signý, Magnus,and the entire Iceland GeoSurvey (ÍSOR) staff: truly, thank you very much for your indisputable guidance throughout, amidst your busy schedules; your level of professionalism and patience with me during the training is totally incredible.

I must frankly acknowledge my employer, Geothermal Development Company (GDC) and, in particular, the Chief Executive Officer, Dr. Silas Simiyu, for nominating and granting me permission to attend this dynamic and informative course; this can never be a waste, I am a more equipped geothermist.

My most profound gratefulness goes to my caring family and friends back home in Kenya for their reassurance and prayers, and for being tolerant of my absence. To my charming husband, Daniel, I am forever indebted to you for believing in me and encouraging me to go for this course; you are so resilient, kind and influential, you have a big room in my heart.

2014 UNU Fellows, you are an awesome company that has kept me going strong. For the light moments and ideas we shared, I say a big thank you. To the Borehole Geology Class 2014, yours is a more exceptional case; together we endured and the special harmony we had is outstanding. Words can never be enough to thank you all.

To my working colleagues back in Kenya, I am also grateful for according me great support, encouragement and advice in various aspects. Just to mention a few, Lucy, Loice, Jeremy and Gerald, you are wonderful guys in my life.

Lastly, I would not have made it were it not for God's divine mercies and sufficient grace, He has been, and forever will be, my supreme source of strength, to Him be all the glory.

REFERENCES

Ali Kassim, M., Carmignani, L., Conti, P., and Fantozzi, P.L., 2002: Geology of the Mesozoic-Tertiary sedimentary basins in southwestern Somalia. *J. African Earth Sciences 34,* 3-20.

Baker, B.H., and Wohlenberg, J., 1971: Structural evolution of the Kenya Rift Valley. *Nature, 229,* 538-542.

Baker, B.H., Mitchell, J.G., and Williams, L.A.J., 1988: Stratigraphy, geochronology and volcano-tectonic evolution of the Kedong-Naivasha-Kinangop region, Gregory Rift Valley, Kenya. *J. Geol. Soc. London, 145,* 107–116.

BGR, 2009: Geothermal exploration at Menengai-Ol'banita prospect. BGR, Germany, website: *www.bgr.bund.de.*

Bosworth, W., Lambiase, J., and Keisler, R., 1986: A new look at Gregory's Rift: The structural style of continental rifting. *Eos, 67,* 577–583.

Chorowicz. J., 2005: The East African Rift System. *J. African Earth Sciences, 43,* 379-410.

Crossley, R., 1979: The Cenozoic stratigraphy and structure of the western part of the rift valley in southern Kenya. *J. Geol. Soc. London, 136,* 393-405.

Dixey, F., 1946: Erosion and tectonics in the east African system. *Quart. J. Geolog. Soc. London, 102,* 339–388.

Franzson, H., 2014: *Petrographic analysis of hydrothermal minerals in thermal reservoirs.* UNU-GTP, Iceland, unpubl. lecture notes.

GDC, 2010: *Menengai geothermal prospect, an investigation for its geothermal potential.* GDC, Nakuru, Kenya, Geothermal Resource Assessment Project, internal report.

GDC, 2013a: *Borehole geological report of well MW-01.* GDC, Nakuru, Kenya, internal report, 16 pp.

GDC, 2013b: *MW-13, preliminary discharge test report.* GDC, Nakuru, Kenya, internal report, 1 pp.

Geotermica Italiana Srl., 1987: *Geothermal reconnaissance survey in the Menengai-Bogoria area of the Kenya Rift Valley.* UN(DTCD)/Government of Kenya, report.

Gichira, J.M., 2012: Joint 1D inversion of MT and TEM data from Menengai geothermal field, Kenya. Report 11 in: *Geothermal training in Iceland 2011.* UNU-GTP, Iceland, 137-167.

Guiraud, R., and Bosworth, W., 1999: Phanerozoic geodynamic evolution of north-eastern Africa and the north-western Arabian platform. *Tectonophysics, 315,* 73–108.

Guiraud, R., Bosworth, W., Thierry, J., and Delplanque, A., 2005: Phanerozoic geological evolution of northern and central Africa: an overview. *J. African Sciences, 43,* 83-143.

Harvey, C., and Browne, P., 2000: Mixed-layer clays in geothermal systems and their effectiveness as mineral geothermometers. *Proceedings of the World Geothermal Congress 2000, Kyushu-Tohoku, Japan*, 1201-1205.

Hetzel, R., and Strecker, M.R., 1994: Late Mozambique belt structures in western Kenya and their influence on the evolution of the Cenozoic Kenya Rift. *J. Structural Geology, 16-2,* 189-201.

Holwell, D.A., Abraham-James, T., Keays, R.R., and Boyce, A.J., 2012: The nature and genesis of marginal Cu–PGE–Au sulfide mineralisation in Paleogene Macrodykes of the Kangerlussuaq region, East Greenland. *Miner. Deposita, 47,* 3-21.

Jones, W.B.,1975: *The geology of the Londiani area of the Kenya Rift Valley*. Univ. of London, UK, PhD thesis, ?? pp.

Jones, W.B., 1985: Discussion on geological evolution of trachytic caldera and volcanology of Menengai volcano, Rift Valley, Kenya. *J. Geol. Soc. London, 142,* 711-712.

Jones, W.B., and Lippard, S.J., 1979: New age determination and geology of Kenya rift – Kavirondo rift junction, west Kenya. *J. Geol. Soc. London, 136*, 63 pp.

KenGen, 2004: *Menengai volcano: Investigations for its geothermal potential.* KenGen, Kenya, Geothermal Resource Assessment Project, unpubl. report.

Kipchumba, J. L., 2013: Borehole geology and hydrothermal alteration of wells MW-08 and MW-11, Menengai geothermal field, Kenya. Report 10 in: *Geothermal training in Iceland 2013*. UNU-GTP, Iceland, 143-176.

Kipng'ok, J., 2011: Fluid chemistry, feed zones and boiling in the first geothermal exploration well at Menengai, Kenya. Report 15 in: *Geothermal training in Iceland 2011*. UNU-GTP, Iceland, 281-302.

Kristmannsdóttir, H., and Tómasson, J., 1978: Zeolite zones in geothermal areas in Iceland. In: Sand, L.B., and Mumpton (editors), *Natural zeolites, occurrence, properties, use*. Pergamon Press Ltd., Oxford, 277-284.

Lagat, J.K., 2004: *Geology, hydrothermal alteration and fluid inclusion studies of the Olkaria Domes geothermal field, Kenya.* University of Iceland, MSc thesis, UNU-GTP, Iceland, report 1, 79 pp.

Leach, T.M., and Muchemi G.G., 1987: Geology and hydrothermal alteration of the North and West exploration wells in the Olkaria geothermal field, Kenya. *Proceedings of the 9th New Zealand Geothermal Workshop, Geothermal Institute, Auckland,* 187-192.

Leat, P.T., 1983: *The structural and geochemical evolution of Menengai caldera volcano, Kenya Rift*

Valley. University of Lancaster, UK, PhD thesis, 482 pp.

Leat, P.T., 1984: Geological evolution of the trachytic caldera volcano Menengai, Kenya Rift Valley. *J. Geol. Soc. London, 141,* 1057-1069.

Leat, P.T., 1991: Volcanological development of Nakuru area of the Kenyan Rift Valley. *J. Afric. Earth Sci., 13*, 483-498.

Leat, P.T., MacDonald, R., and Smith, R.L., 1984: Geochemical evolution of the Menengai caldera volcano, Kenya. *J. Geophys. Res., 89,* 8571-8592.

Lopeyok, T.P., 2013: Borehole geology and hydrothermal mineralization of wells MW-09 and MW-11, Menengai geothermal field, Kenya. Report 15 in: *Geothermal training in Iceland 2013*. UNU-GTP, Iceland, 289-324.

Lynne, B.Y., Campbell, K.A., Perry, R.S., Browne, P.R.L., and Moore, J.N., 2006. Acceleration of sinter diagenesis in an active fumarole, Taupo volcanic zone, New Zealand. *Geology, 34*, 749-752.

MacDonald, R., 2003: Magmatism of the Kenya Rift Valley: a review. *Earth sciences, 93,* 239-253.

MacDonald, R., Bagiński, B., Leat, P.T., White, J.C., and Dzierżanowski, P., 2011: Mineral stability in peralkaline silicic rocks: information from trachytes of the Menengai volcano, Kenya. *Lithos, 125,* 553–568.

MacDonald, R., Belkin, H.E., Fitton, J.G., Rogers, N.W., Nejbert, K., Tindle, A.G., and Marshall, A.S., 2008: The roles of fractional crystallization, magma mixing, crystal mush remobilization and volatile melt interactions in the genesis of a young basalt - peralkaline rhyolite suite, the Greater Olkaria volcanic complex, Kenya Rift Valley. *J. Petrology, 49*, 1520-1530.

Malimo, S.J., 2009: Interpretation of geochemical well test data for wells OW-903B, OW-904B and OW-909, Olkaria Domes field, Kenya. Report 17 in: *Geothermal training in Iceland 2009.* UNU-GTP, Iceland, 336-337.

Mariita, O., and Keller, G., 2007: An integrated geophysical study of the northern Kenya Rift, Kenya. *J. African Earth Sciences, 48,* 80-94.

Marks, N., Schiffman, P., Zierenberg, R.A., Franzson, H., and Fridleifsson, G.Ó., 2009: Hydrothermal alteration in the Reykjanes geothermal system: Insights from Iceland deep drilling program well RN-17. *J. Volcanol. & Geoth. Res., 189-2010,* 172-190.

McCall, G.J.H., 1957: The Menengai caldera, Kenya colony. *Proceedings of the 20th International Geol. Congress, Section 1,* 55-69.

McCall, G.J.H., 1967: *Geology of the Nakuru-Thomson's Falls-Lake Hannington area.* Geological Survey of Kenya, report 78, 122 pp.

Mibei, G., 2012: Geology and hydrothermal alteration of Menengai geothermal field. Case study: Wells MW-04 and MW-05. Report 21 in: *Geothermal training in Iceland 2012.* UNU-GTP, Iceland, 442-448.

Mibei, G.K., and Lagat, J., 2011: Structural controls in Menengai geothermal field. P*roceedings of the Kenya Geothermal Congress 2011, Nairobi, Kenya,* 28-37.

Musonye, X.S., 2012: Borehole geology and alteration mineralogy of well OW-914A, Domes area, Olkaria geothermal field, Central Kenya Rift. Report 23 in: *Geothermal training in Iceland 2012*. UNU-GTP, Iceland, 501-540.

Mwangi, D.W., 2012: Borehole geology and hydrothermal mineralisation of well OW–916, Olkaria Domes geothermal field, Naivasha, Kenya. Report 24: *Geothermal training in Iceland 2012*. UNU-GTP, Iceland, 541-571.

Njathi, D.W., 2012: Borehole geology and hydrothermal mineralisation of well OW-911A, Olkaria Domes geothermal field, Central Kenya Rift Valley. Report 25: *Geothermal training in Iceland 2012*. UNU-GTP, Iceland, 573-600.

Njue, L.M., 2010: Borehole geology and hydrothermal mineralisation of well HE-27, Hellisheidi geothermal field, SW-Iceland. Report 24 in: *Geothermal training in Iceland 2010*. UNU-GTP, Iceland, 493-524.

Okoo, J.A., 2013: Borehole geology and hydrothermal alteration mineralogy of well OW-39A, Olkaria geothermal project, Naivasha, Kenya. Report 24 in: *Geothermal training in Iceland 2013*. UNU-GTP, Iceland, 547-576.

Omenda, P.A., 1998: The geology and structural controls of the Olkaria geothermal system, Kenya. *Geothermics, 27-1*, 125–130.

Otieno, V. and Kubai, R., 2013: Borehole Geology and Hydrothermal Mineralisation of Well OW-37A, Olkaria East Geothermal Field, Kenya. Report 2 in: *Geothermal Training in Kenya 2012 – 2013*, 105 pp.

Reyes, A.G., 2000: *Petrology and mineral alteration in hydrothermal systems. From diagenesis to volcanic catastrophes.* UNU-GTP, Iceland, report 18, 1998, 77 pp.

RockWare, 2007: *LogPlot Program*. RockWare, Inc., USA.

Roedder, E., 1984: *Fluid inclusions*. Mineral. Soc. Am., Rev. Mineral., 12, Washington, DC, 7 pp.

Rogers, N., Macdonald, R., Fitton, G.J., Smith, M., and Barreino, B., 2000: Two mantle plumes beneath the East African rift system: Sr, Nd and Pb isotope evidence from Kenya Rift basalts. *Earth & Planetary Sci. Letters, 176-3/4,* 387-400.

Ronoh, I.J., 2012: Borehole geology and hydrothermal alteration of well OW-912B, Olkaria Geothermal field, Central Kenya Rift Valley. Report 29 in: *Geothermal training in Iceland 2012*. UNU-GTP, Iceland, 695-732.

Saemundsson, K., and Gunnlaugsson, E., 2014: *Icelandic rocks and minerals* (2nd ed.). Forlagið ehf and Reykjavik.

Simiyu, S.M., 1999: Seismic velocity analysis in the Olkaria geothermal field. *Proceedings of the 24th Workshop on Geothermal Reservoir Engineering, Stanford University, Stanford,* 6 pp.

Simiyu, S.M., and Keller, G.R., 1997: Integrated geophysical analysis of the East African plateau from gravity anomalies and recent seismic studies. *Tectonophysics, 278,* 291–314.

Simiyu, S.M., and Keller, G.R., 2001: An integrated geophysical analysis of the upper crust of the southern Kenya Rift. *Geophys. J. Int. 147,* 543-561.

Smith, M., and Mosley, P., 1993: Crustal heterogeneity and basement influence on the development of the Kenya Rift, East Africa. *Tectonics, 12,* 591-606.

Strecker, M.R., and Melnick, D., 2013: *Structural characteristics of Menengai caldera, central Kenya Rift, Republic of Kenya: preliminary assessment of the structural characteristics of Menengai caldera and regions farther north, Nakuru, Kenya.* GDC, Kenya, unpublished report.

Tole, M.P., 1996: Geothermal energy research in Kenya: a review. *J. African Earth Sci., 23,* 565-575.

Wamalwa, A.M., 2011: *Joint geophysical data analysis for geothermal energy exploration*. University of Texas, El Paso, Tx, PhD thesis, 101 pp.

Vaughan, D.J., 2006: Sulphide mineralogy and geochemistry, vol. 61, description. Mineralogical Society of America., website: *www.minsocam.org/msa/rim/Rim61.html.*

APPENDIX I: Typical XRD patterns for smectite and illite clay minerals in well MW-13

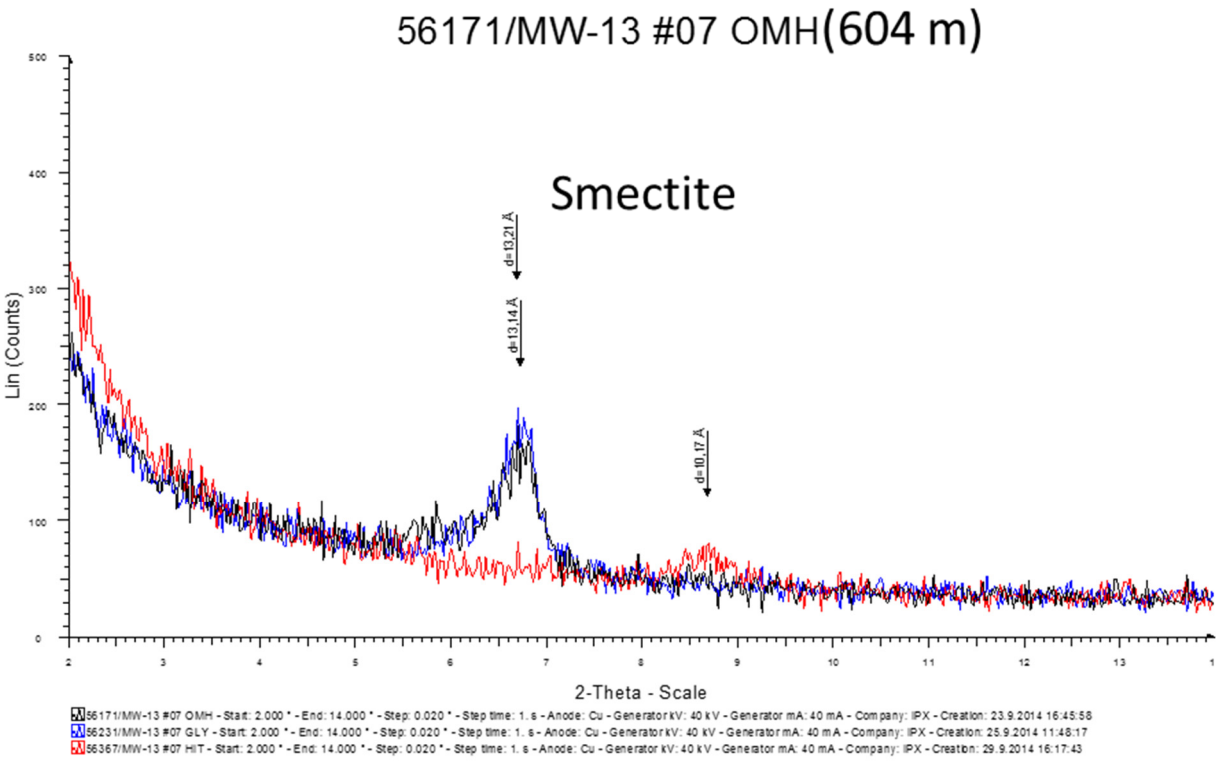

FIGURE 1: Smectite clay at 604 m, well MW-13

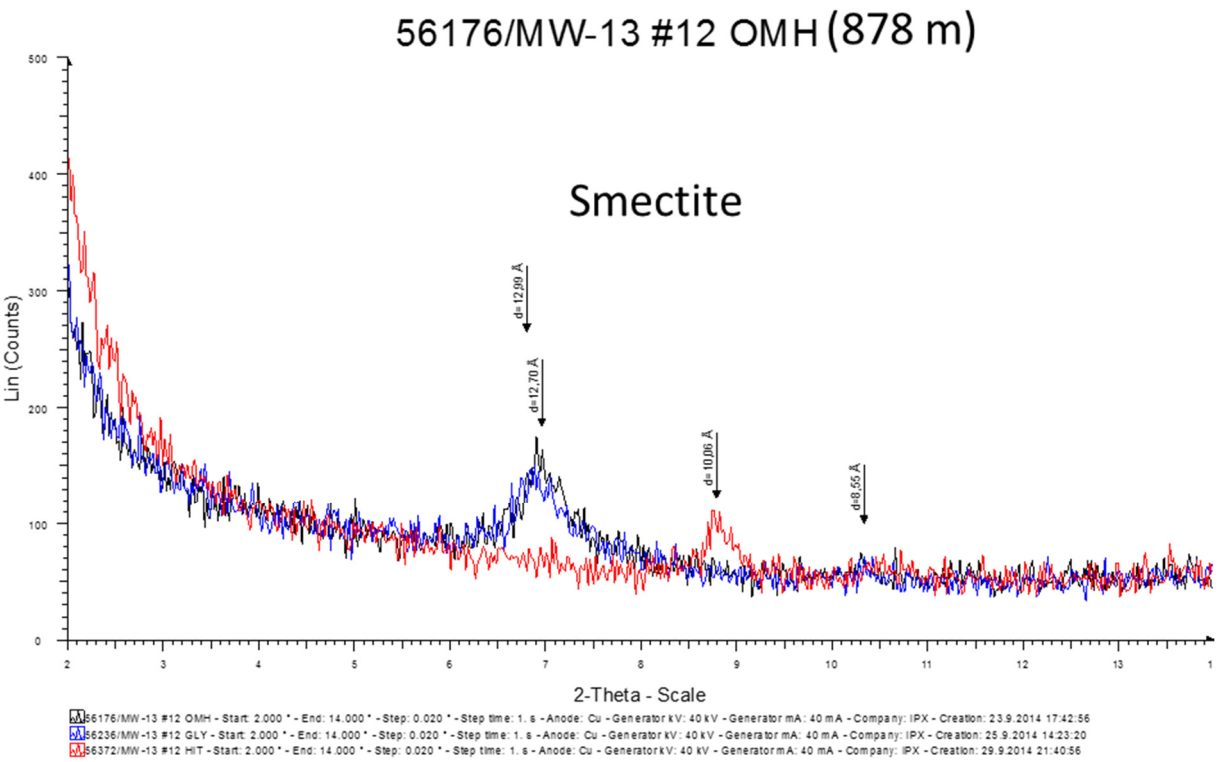

FIGURE 2: Smectite clay at 878 m, well MW-13

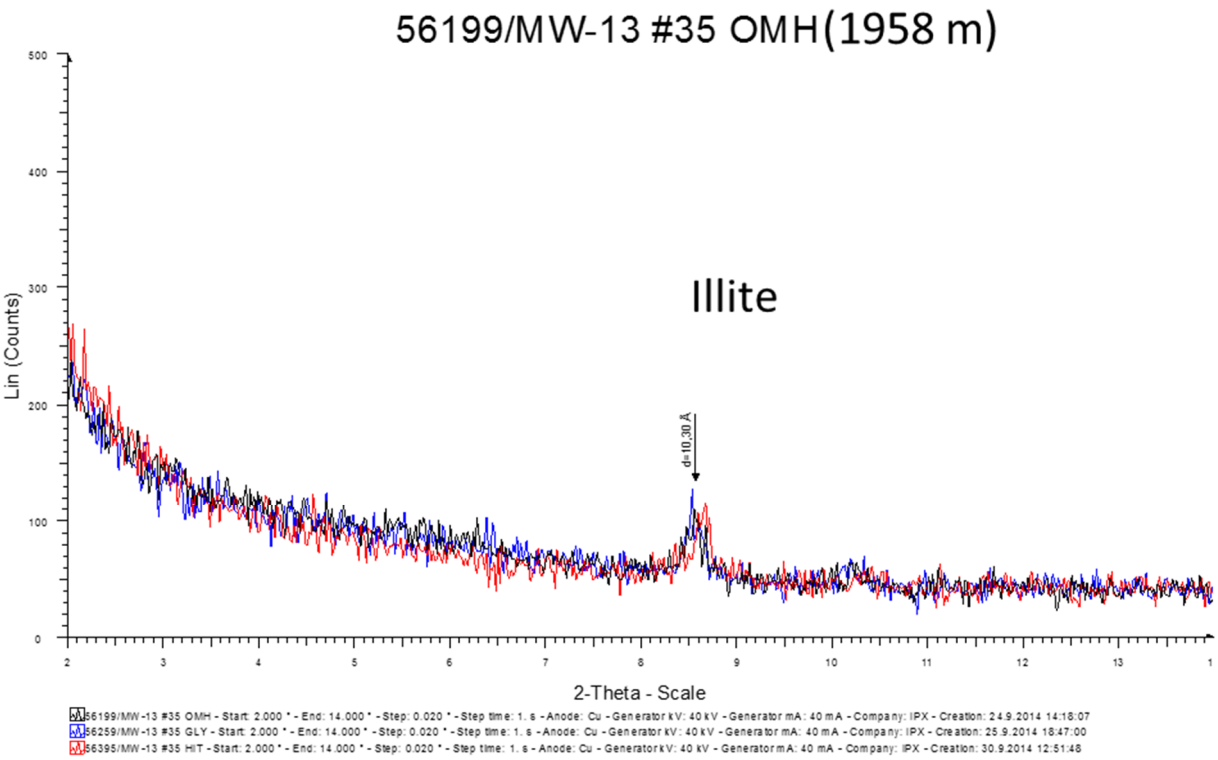

FIGURE 3: Illite clay at 1958 m, well MW-13